Check for updates

Received: 19 July 2024 | Revised: 17 September 2025 | Accepted: 8 October 2025

DOI: 10.1111/joa.70059

Journal of Anatomy ANATOMICAL SOCIETY WILEY

ORIGINAL ARTICLE

Tooth–bone attachment tissue is produced by cells with a mixture of odontoblastic and osteoblastic features in reptiles

M. Šulcová[1,2] | J. Dumková[3] | B. Hutečková[1,2] | M. Kavková[4] | V. Parobková[4] | O. Zahradníček[5] | J. Křivánek[3] | I. Adameyko[6,7] | J. Kaiser[4] | T. Zikmund[4] | A. S. Tucker[8] | M. Buchtová[1,2]

[1]Department of Experimental Biology, Faculty of Science, Masaryk University, Brno, Czech Republic

[2]Laboratory of Molecular Morphogenesis, Institute of Animal Physiology and Genetics, v.v.i., Czech Academy of Sciences, Brno, Czech Republic

[3]Department of Histology and Embryology, Faculty of Medicine, Masaryk University, Brno, Czech Republic

[4]Central European Institute of Technology, Brno University of Technology, Brno, Czech Republic

[5]Department of Radiation Dosimetry, Nuclear Physics Institute, Czech Academy of Sciences, Prague, Czech Republic

[6]Department of Neuroimmunology, Center for Brain Research, Medical University of Vienna, Vienna, Austria

[7]Department of Physiology and Pharmacology, Karolinska Institutet, Stockholm, Sweden

[8]Centre for Craniofacial and Regenerative Biology, Floor 27 Guy's Tower, Guy's Hospital, King's College London, London, UK

Correspondence
M. Buchtová, Laboratory of Molecular Morphogenesis, Institute of Animal Physiology and Genetics, v.v.i., Czech Academy of Sciences, Veveri 97, 602 00 Brno, Czech Republic.
Email: buchtova@iach.cz

Funding information
Grantová Agentura České Republiky, Grant/Award Number: 22-02794S; Ministerstvo Zdravotnictví Ceské Republiky, Grant/Award Number: NW24-10-00204; Ministerstvo Školství, Mládeže a Tělovýchovy, Grant/Award Number: CZ.02.01.01/00/22_008/0004593, CZ.02.1.01/0.0/0.0/15_003/0000460, CZ.02.1.01/0.0/0.0/16_019/0000728 and LM2023050

Abstract

Teeth are anchored in the jaw in a highly variable manner across vertebrates. In mammals and crocodiles, the teeth are cushioned inside bony sockets by periodontal ligaments, whereas most squamate reptiles have teeth firmly attached to the jawbone. Here, we analyzed the development of the attachment tissue in the veiled chameleon, a species with firm acrodont tooth attachment, to reveal the cellular processes establishing ankylosis and to determine the cell types contributing to the attachment. The tooth-bearing bones formed pedicles with edges fusing to the dentine via an attachment tissue produced by morphologically distinct cells exhibiting both osteoblastic and odontoblastic features. These cells were RUNX2-positive, suggesting their potential to differentiate into hard-tissue-producing cells. However, in contrast to the osteoblasts of the bony pedicles, tooth–bone interface (TBI) cells expressed elevated levels of Na^+-/K^+-ATPase and thus resembled odontoblasts. TBI cells were visible only temporarily, and after tooth–bone fusion they were removed by apoptosis and phagocytosis. Dynamic deposition of the hard matrix continued on both sides of the TBI and during the posthatching stages through the participation of osteoblasts. Overall, our findings demonstrate both odontoblast- and osteoblast-like characteristics of cells producing the attachment tissue at the TBI during development in chameleons, highlighting the existence of a transient intermediate cell population, which we call ankyloblasts.

KEYWORDS
acrodont dentition, Calbindin1, odontoblasts, osteoblasts, reptiles, Runx2, teeth

This is an open access article under the terms of the Creative Commons Attribution-NonCommercial License, which permits use, distribution and reproduction in any medium, provided the original work is properly cited and is not used for commercial purposes.
© 2025 The Author(s). *Journal of Anatomy* published by John Wiley & Sons Ltd on behalf of Anatomical Society.

1 | INTRODUCTION

Several types of tooth–bone attachment have evolved in different branches of amniotes. The most studied type of tooth anchorage is thecodont implantation, characterized by a nonmineralized periodontal ligament linking the tooth to the jawbone inside a deep alveolus (Bertin et al., 2018; Diekwisch, 2001). This attachment, called gomphosis, is present in mammals and crocodilians and provides robust resistance to mechanical stress during food processing (McIntosh et al., 2002).

By contrast, the teeth of recent lepidosaurian reptiles are firmly attached to the jaw bones, although the morphology of this type of attachment varies across species (Gaengler, 2000). In most lizards and snakes, teeth are ankylosed to the inner side of the high labial wall of the jawbone (pleurodont attachment). However, in some species (e.g., agamas, chameleons), the teeth are completely fused to the crest of the tooth-bearing bone (acrodont teeth) (Edmund, 1960). Such cases, where the teeth are firmly fused to the tooth-bearing element by mineralized tissue, are called ankylosis (for nomenclature, see a recent review by Bertin et al., 2018). Although ankylosis is widespread in nature, in mammals, a fusion of the tooth to the bone by hard tissue is considered a pathological condition (Palone et al., 2020; Tong et al., 2020).

Diverse developmental mechanisms have been proposed to explain the evolutionary origin and elaboration of ankylosis. The first developmental step of ankylosis is described as a soft ligament mineralization (LeBlanc et al., 2016; Liu et al., 2016). The periodontal ligaments in ancestral mammals have been predicted to display a high osteogenic potential, with an inclination to become calcified, thus resulting in dental ankylosis (LeBlanc et al., 2016). The mineralized ligamentous tissue has been preserved in fossilized mosasaurs, and it is also evident in several fish species and modern snakes (LeBlanc, Lamoureux, & Caldwell, 2017; Luan et al., 2009; Peyer, 1968). In the second type, ankylosis has been described as developing without ligament formation, with the tooth base firmly attached directly to the top of the tooth-bearing bony pedicles with no sign of previous ligament production (Buchtová et al., 2013; Luan et al., 2009). In both scenarios, the bridge between the bone and the tooth can be formed by a mineralized tissue, which is called the "attachment bone" (Luan et al., 2009). However, the nature of tooth attachment tissue varies depending on the species and the mode of attachment, with various tissues described to be involved in its formation, including cementum, dentine, and alveolar bone (Bertin et al., 2018). In addition, an abundance of intermediate tissues such as osteodentin, dentin with enclosed odontoblasts, atubular dentine, acellular bone, acellular cementum, or cartilaginous tooth cementum has been described as contributing to attachment between the tooth and bone (Caldwell et al., 2003; Edmund, 1969; Howes, 1979; LeBlanc et al., 2016; LeBlanc, Lamoureux, & Caldwell, 2017; Listgarten & Shapiro, 1974; Luan et al., 2009; Meunier, 2015; Peyer, 1968; Rieppel, 2001; Rieppel & Kearney, 2005; Zaher & Rieppel, 1999).

Here, we aim to reveal the progress of developmental features underlying the formation of the tooth–bone interface (TBI) in the veiled chameleon to understand the process of attachment during ankylosis over time. Chameleon teeth are located on the crest of the tooth-bearing bones, and they are attached to the underlying bone by acrodont ankylosis (Dosedělová et al., 2016) and undergo similar developmental stages during odontogenesis to those described for mammalian species (Buchtová et al., 2013; Kavková et al., 2020; Luckett, 1993). We followed TBI development from its initiation, when the tooth and bone first approached each other, to the stage at which the TBI-forming cells produced the connecting mineralized tissue. The TBI cells were evaluated at the ultrastructural, cellular, and molecular levels to assess their identity and the characteristics of the final attachment tissue. Moreover, the cellular processes of the TBI were systemically analyzed to follow the rearrangement and remodeling of the TBI-related skeletal elements during development.

2 | MATERIALS AND METHODS

2.1 | Experimental animals

Fertilized eggs of the veiled chameleon (*Chamaeleo calyptratus*) were obtained from commercial breeders. To analyze developmental processes during the pre- and posthatching stages, eggs were incubated in an incubator, maintaining a temperature not exceeding 29°C. At the designated time points, eggs were collected and carefully opened to access the embryos, which were then euthanized through decapitation (Table S1). The eggs of *Anolis allisoni* were obtained from a private breeder and were sacrificed in the later stage of embryonic development by low temperature and decapitation. Juveniles of *Cryptelytrops albolabris*, already fixed in 10% formaldehyde, were also obtained from a private breeder. They were euthanatized by low temperature and then decapitated before tissue fixation. All animal procedures adhered to the ethical guidelines established by the Laboratory Animal Science Committee of Masaryk University (Brno, Czech Republic, MSMT-10946/2021-5).

2.2 | Processing of tissues for histological analyses

To facilitate immunohistochemical and histological analyses, heads dissected from specimens were fixed in 4% PFA overnight at +4°C. For older specimens, tissues were decalcified in 12.5% EDTA in 4% PFA at room temperature for a period ranging from 3 weeks to 2 months, depending on the extent of tissue mineralization. Following fixation and/or decalcification, specimens underwent dehydration in an ethanol and xylene series, followed by embedding in paraffin wax. Then, a series of transversal histological sections (5 μm thick) were prepared. Selected sections were stained with Hematoxylin-Eosin or Sirius Red to analyze collagen fibers.

14697580, 2026, 2, Downloaded from https://onlinelibrary.wiley.com/doi/10.1111/joa.70059 by Brno University Of Technology, Wiley Online Library on [31/03/2026]. See the Terms and Conditions (https://onlinelibrary.wiley.com/terms-and-conditions) on Wiley Online Library for rules of use; OA articles are governed by the applicable Creative Commons License

2.3 | Immunohistochemical labeling

Alternative sections of paraffin-embedded tissues were used for immunohistochemical analysis of protein expression. The initial steps involved deparaffinization in xylenes, and rehydration through an ethanol series was performed. Epitopes were unmasked by antigen retrieval in citrate buffer (pH 6) for 15 min in a water bath (97°C). Blocking serum was applied directly on the samples to prevent nonspecific antibody binding and incubated with serum for 30 min. Primary antibodies (Calbindin1, RUNX2, pan-cytokeratin, Na^+-/K^+-ATPase) were applied to the slides and incubated for 1 h (refer to Table S2 for information about the primary antibodies used).

To detect Calbindin1 and Na^+-/K^+-ATPase, a secondary antibody (donkey anti-rabbit Alexa Fluor 555, cat. no. A31572, Thermo Fisher, USA) conjugated with fluorochrome was used with an incubation time of 30 min. For nuclei visualization, either DRAQ5™ Fluorescent Probe Solution (cat. no. 62251, ThermoFisher, USA) or Fluoroshield with DAPI (cat. no. F6057, Sigma–Aldrich, St. Louis, Missouri) was applied. Images were captured using a fluorescent microscope Leica DM LB2 or a confocal microscope Leica SP8 using 20× objectives (Leica Microsystems, Germany) with Leica Application Suite software. Processing of images was conducted using IMARIS software (Bitplane, Zürich, Switzerland) or Adobe Photoshop 7.0 (USA).

To detect RUNX2, pan-cytokeratin, and CD68, a secondary biotinylated anti-rabbit antibody (1:200, part of the ABC kit, Vectastain, Vector Laboratories, Burlingame, USA) was applied for 30 min, followed by the application of avidin–biotin complex (ABC kit, Vectastain, Vector Laboratories, Burlingame, USA) for an additional 30 min. The signal was visualized with diaminobenzidine (DAB), and slides were counterstained with Hematoxylin to visualize nuclei. Stained samples were photographed using a Leica DM2500LED (Leica Microsystems, Wetzlar, Germany).

2.4 | TUNEL assay

The presence of apoptotic cells was determined by detecting DNA fragments using a TUNEL assay (ApopTag Peroxidase in Situ Apoptosis Detection Kit-S7101, Chemicon, Temecula, USA). Hematoxylin was used to counterstain nuclei. Photomicrographs of the sections were captured under bright-field illumination with a Leica DM2500LED (Leica Microsystems, Wetzlar, Germany).

2.5 | TRAP assay

For the detection of tartrate-resistant acid phosphatase (TRAP) in osteoclasts, a mixture of the following solutions was used: Naphtol AS-TR phosphate disodium salt (0.0023 M, cat. no. N6125, Sigma–Aldrich, Germany), *N*,*N*-dimethylformamide (0.5%), glacial acetic acid (0.2 M), sodium acetate (0.2 M), sodium tartrate dibasic dihydrate (0.1 M, cat. no. S-8640, Sigma–Aldrich, Germany), Fast Red TR Salt (0.1%, cat. no. 368881, Sigma–Aldrich). The pH of the solution was adjusted to 4.3.

Once the mixture was prepared, it was added to preheated slides at 37°C for 1 h at 37°C. Following the incubation, Hematoxylin staining was used as a counterstain, and images were captured using a Leica DM2500LED microscope (Leica Microsystems, Wetzlar, Germany).

2.6 | In vivo injection of Calcein Green and Alizarine Red into juvenile chameleons

Fertilized eggs were incubated at 28–29°C until hatching. Juveniles were housed in cages with a UVA and UVB light source and received regular cricket feedings. Humidity levels were maintained through periodic water spraying.

After 2 months, two groups (each containing four animals) were injected with Calcein Green (cat. no. C0875-5G, Sigma–Aldrich) and Alizarin Red (cat. no. A533-25g, Sigma–Aldrich) to monitor the dynamics of hard-tissue deposition. Selected fluorescent dyes were diluted in 2% $NaHCO_3$ (pH 7.4, 30067-AP0-G0500-1, Lach-Ner) at concentrations of 6 mg/kg for Calcein Green and 30 mg/kg for Alizarin Red with a final volume of 50 µL injected into each animal.

One group of animals was injected intraperitoneally with Calcein Green on day one, followed by Alizarin Red after 3 days, and the animals were euthanized 3 days later. The second group was injected with Calcein Green on the same day as the first group, but Alizarin Red was injected after 6 days. Animals from the second group were sacrificed after another 6 days by decapitation. This allowed for the assessment of two different time points to observe the dynamic process of hard tissue deposition. The selected time range of 3 and/or 6 days was selected according to similar experiments performed previously (Gonzalez Lopez et al., 2023). Lower jaws of the specimens from each group were dissected out, fixed in 10% PFA for 3 days, put in 30% Sucrose (cat. no. S0389, Sigma–Aldrich) overnight, embedded in frozen section media (cat. no. 3801480, Leica Biosystems), sectioned on a Leica cryostat, and then sections were collected on Japanese tape (Cryofilm type III C(16UF), SECTION-LAB Co. Ltd, Japan).

Cryosections (10 µm) through the jaw were washed in PBS-T, mounted in Fluoroshield (cat. no. F6057, Sigma–Aldrich, St. Louis, Missouri), and imaged on a Leica SP8 confocal microscope (Leica Microsystems, Wetzlar, Germany). Whole-mount images were obtained using the BEE-ST (Bones and tEEth Spatio-T, Bemporal growth monitoring) approach (Gonzalez Lopez et al., 2023).

2.7 | Transmission electron microscopy

Individually dissected jaws were fixed in 3% glutaraldehyde buffered with 0.1 M cacodylate buffer for 24 h. We used nondemineralized preparations to preserve the mineralized context of the tissue and to avoid artifacts associated with demineralization, which is critical for accurate interpretation of cell–matrix interactions and mineral deposition.

14697580, 2026, 2, Downloaded from https://onlinelibrary.wiley.com/doi/10.1111/joa.70059 by Brno University Of Technology, Wiley Online Library on [31/03/2026]. See the Terms and Conditions (https://onlinelibrary.wiley.com/terms-and-conditions) on Wiley Online Library for rules of use; OA articles are governed by the applicable Creative Commons License

This was followed by three washes in 0.1 M cacodylate buffer and postfixation in 1% OsO_4 solution for 1 h. After additional washing in 0.1 M cacodylate buffer, the samples were dehydrated through increasing ethanol concentrations followed by acetone and embedded in the epoxy resin Durcupan.

First, we prepared semithin sections stained with Toluidine Blue that offer an intermediate resolution of tissue structure. These images are presented alongside, or in some cases instead of, selected TEM panels to improve clarity and facilitate interpretation of the developmental processes.

For each sample, an average of four TEM grids, each containing two to four sections, was generated using a Leica EM UC6 ultramicrotome (Leica Mikrosysteme GmbH, Vienna, Austria). The sections were placed on formvar-coated nickel grids; half of them were contrasted with lead citrate and uranyl acetate, and the other half was analyzed without this additional contrast.

The ultrastructure analyses of all samples were conducted using the Morgagni™ 268 TEM (FEI Company, Eindhoven, Netherlands) with photographs captured using a Veleta CCD camera (Olympus, Münster, Germany). Distances between selected structures were measured using iTEM software (FEI Company, Eindhoven, Netherlands).

2.8 | Micro-CT analyses

Five samples of embryonic chameleon jaws underwent micro-CT analysis to examine the hard-tissue morphology (Table S3). The samples were embedded in 1% agarose gel within 500 µL Eppendorf tubes to mitigate potential movement during scanning. X-ray microcomputed tomography (micro-CT) measurements were performed using the GE Phoenix v|tome|x L 240 laboratory system (GE Sensing & Inspection Technologies GmbH, Germany).

This system is equipped with a high-contrast flat panel detector (dynamic 41|100, 4000×4000 pixels with a pixel size of 100 µm) and a nanofocus X-ray tube (180 kV/15 W maximum power). The micro-CT system operated within an air-conditioned cabinet, and all measurements were performed at a controlled temperature of 21°C. Acquisition parameters were individually optimized for each sample to achieve the best possible voxel size (Table S3), which ranged from 2.0 to 3.5 µm depending on the specimen's size and developmental stage. The spatial resolution was roughly twice the voxel size, consistent with the Nyquist criterion. Tomographic reconstruction was performed using GE Phoenix datos|x 2.0 software (GE Sensing & Inspection Technologies GmbH, Germany), and the image processing, along with analysis and visualization, was performed using VG Studio MAX 3.3 software (Volume Graphics GmbH, Germany).

Wall thickness was quantified in VG Studio MAX using the sphere method, which estimates local thickness by fitting the largest possible sphere between the inner and outer surfaces of a structure at each point. The diameter of this sphere represents the thickness at that location. The resulting thickness measurements were visualized in a 3D color-coded map, where cooler colors (e.g., blue) indicate thinner regions and warmer colors (e.g., red) indicate thicker areas, facilitating intuitive assessment of spatial thickness variations within the sample.

3 | RESULTS

3.1 | Interaction between the developing tooth germ and bone pedicle is initiated at the bell stage

At the early bell stage of chameleon tooth development, mineralization was evident at the tip of the cusps (Figure 1a,b), with the cervical loops extending down around the forming dental papilla (Figure 1b). At this "Initiation of interface formation" stage (IF stage—stage 1 of TBI formation), the bony pedicle was at a distance (approximately 20 µm) from the tooth germ (Figure 1a′). However, a distinct group

FIGURE 1 Tooth–bone interface development and its morphology during early stages of odontogenesis. (a) At the early mineralization stage, hard tissue deposition had started in the jawbone and tooth areas. Micro-CT scan displays tips of the central cusp already covered by mineralized tissue. Deposition has also initiated in lateral cusps (a, black arrowhead). There was a large gap between hard tissues in the TBI area (white arrow). (a′, a″) Extensive communication between dental pulp and jawbone marrow can be seen on the lateral (a′) and dorsal view (a″) of the lower jaw, including bone lamella (bl) separating them. (b, b′, b″) Several preosteoblast cells overhung the area between the developing tooth germ and bone on both sides of the tooth in microscopic sections stained by Hematoxylin–Eosin (black outlines in (b′), (b″), and (f) detail in TEM). (c) Cells of future TBI area (arrowheads) were RUNX2-positive (c′—detail of labial part of cervical loop, c″—detail of lingual part of cervical loop). (d–i) The nature of cells, which were expanding from bone pedicles in TEM. (d) Semithin section of the tooth stained by Toluidin Blue. (e) Ultrathin section through cervical loop (cl) and odontoblast layer (od) outlaying the edge of cervical loop. (f–i) Labial part of the cervical loop with preosteoblasts (ob) extending by long cellular processes (arrowhead) from the cervical loop (cl) toward bone pedicle (bp). (g–i) High power view of the labial side of the bone pedicle with distinct bone matrix (b). (j–j″) Later, when the bone and dentine approached each other, the bone pedicles (bp) were the largest at the labial and lingual side of the jaw, therefore forming the walls protruding along the jaw (j″, arrowheads). As the mineralization proceeded, bone lamellae (bl) expanded to separate the bone marrow from the dental pulp, and the communication holes became smaller (j″, arrowheads). (k–k″) The epithelium of the cervical loop's labial and lingual parts was getting close to extending bone pedicles, as apparent from the Hematoxylin–Eosin. There were differences between the labial and lingual parts of the cervical loop, with the labial epithelium outgrowing inwards the dental pulp (k′). The lingual part of the cervical loop extended to exceed the labial bone pedicle (k″). (l–l″) RUNX2-positive cells were located in the surrounding TBI around the cervical loop. (m) Osteoclasts were not apparent at the very top of bone pedicles. Instead, they were situated around the bony lamella and along the inner side of the bone, facing the jawbone marrow (arrowheads). (n) Few apoptotic cells were located in the mesenchyme between bone pedicles and the cervical loop (inset).

14697580, 2026, 2, Downloaded from https://onlinelibrary.wiley.com/doi/10.1111/joa.70059 by Brno University Of Technology, Wiley Online Library on [31/03/2026]. See the Terms and Conditions (https://onlinelibrary.wiley.com/terms-and-conditions) on Wiley Online Library for rules of use; OA articles are governed by the applicable Creative Commons License

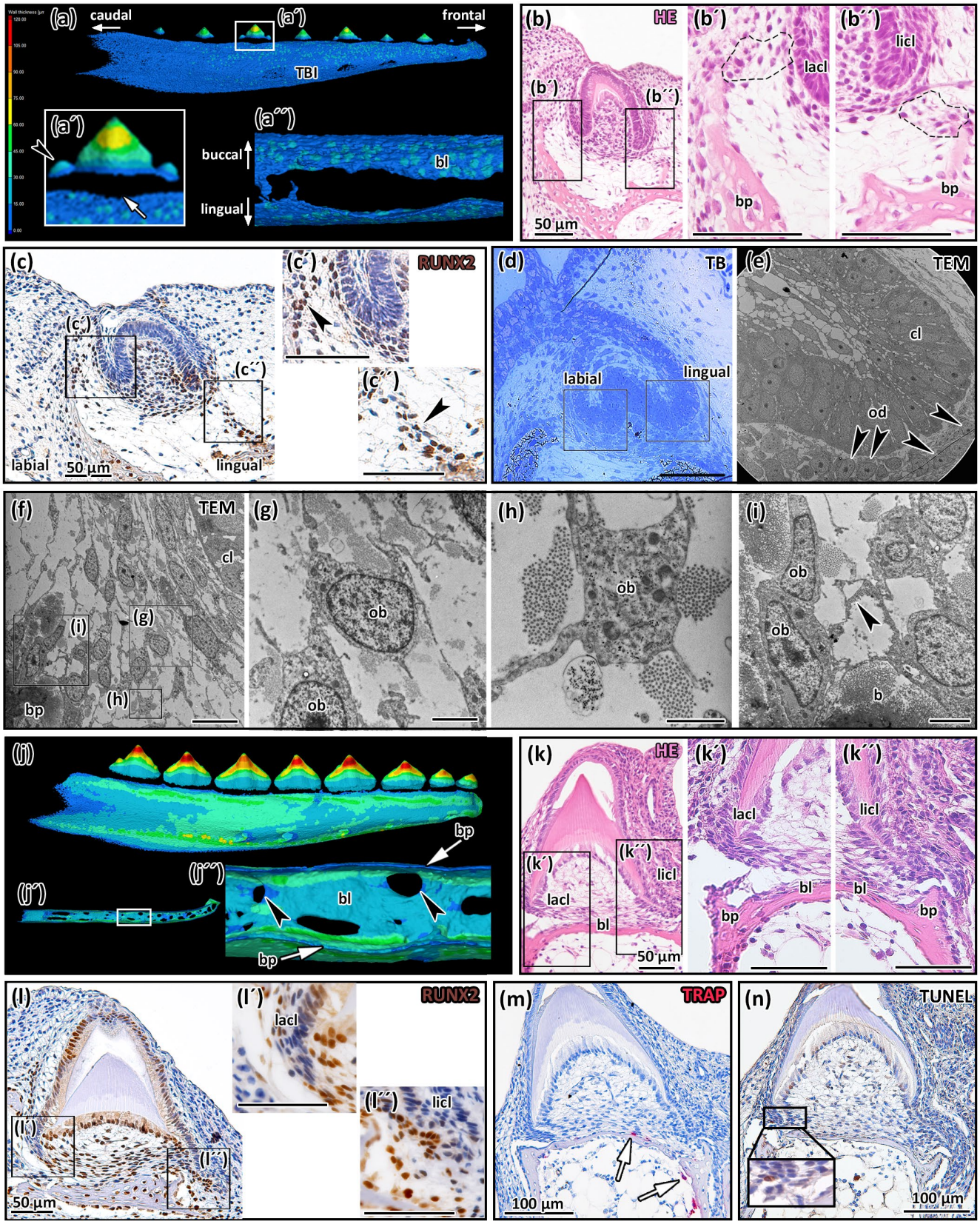

of mesenchymal cells was evident spanning the gap between the tooth and bone on either side of the tooth (Figure 1b,b′,b″). To understand the identity of these cells, we analyzed the expression of RUNX2 (CBFA1), a classic osteoblast and odontoblast marker, that also shows later expression in differentiating ameloblasts (Ducy et al., 1997; Lian et al., 2006). Interestingly, in addition to expression in the osteoblasts lining the bone, odontoblasts within the dental papilla, and in the forming ameloblasts of the dental epithelium, the

14697580, 2026, 2, Downloaded from https://onlinelibrary.wiley.com/doi/10.1111/joa.70059 by Brno University Of Technology, Wiley Online Library on [31/03/2026]. See the Terms and Conditions (https://onlinelibrary.wiley.com/terms-and-conditions) on Wiley Online Library for rules of use; OA articles are governed by the applicable Creative Commons License

linking cells were also RUNX2-positive, in contrast to the mesenchyme flanking these regions (Figure 1c,c′, see also Figure S1). This suggests that these cells might have the potential to differentiate into cells that secrete hard tissue. TEM was used to follow their ultrastructural morphology to understand the nature of these cells in more detail (Figure 1e–i, Figure S2a–h). Mesenchymal cells in the dental papilla, and around the tip of the cervical loop, exhibited features of polarized cuboid preodontoblasts (Figure 1d,e). Cells located outside of the tooth on the tip of the growing cervical loop were connected by long cytoplasmic processes (Figure 1f,g). These processes were directed toward the forming bone pedicles, indicating very early establishment of interactions between the bone and tooth. Collagen fibril deposition was evident, with fibrils organized into bundles parallel to the jaw's long axis (Figure 1h,i; Figure S1a–d). These outer cells demonstrated osteoblast-like morphologies, with dilated cisternae of the rough endoplasmic reticulum (Figure 1g,i) and an increased nucleocytoplasmic ratio compared to the inner cells. In summary, both odontoblast-like (located close to the epithelium) and osteoblast-like (located further from the tooth, closer to the forming bone pedicles) cells were associated with the initiation of the TBI area.

As the tooth developed, the TBI narrowed (Figure 1j–n), and the tooth germs elongated toward the growing bone pedicle (Figure 1k,k′,k″). Bone lamellae separated the bone marrow from the dental papilla, but communication would still be possible due to the presence of large connecting channels (black arrow in Figure 1j″). Both osteoblasts and odontoblasts produced hard tissue. The RUNX2-expressing cells were located between the forming tooth and bone as the cervical loop of the tooth extended close to the bone (Figure 1l,l′; Figure S1a–d). We call this stage the "Hard-tissue rearrangement stage" (HTR stage—stage 2 of TBI formation). During this stage, TRAP-positive osteoclasts were evident in close contact with the bone but were not associated with the forming tooth–bone interface area (Figure 1m, Figure S3a–h). Several mesenchymal cells in the forming TBI area were TUNEL-positive (Figure 1n, Figure S3k–r), indicating cell clearance by apoptosis in this area before tooth–bone fusion.

3.2 | Establishment of direct contact between the dentine and bony pedicles is mediated by a group of cells with intermediate characteristics

As the tooth developed further, the tooth and bone came into close contact (Figure 2a,a′,b,b′,b″). This stage was called the "Attachment tissue production stage" (ATP stage—stage 3 of TBI formation). The bony pedicles were extended along the jaw but were still very short and thin (Figure 2a′,a″). Under the pedicles, the bones were thickened as visualized by wall thickness analyses (yellow spots in wall thickness analyses) (Figure 2a″), and small dental channels connected the bone marrow with the dental pulp (arrow in Figure 2a″).

The dentine was tightly covered by the dental epithelium as labelled by pan-cytokeratin, with the epithelium of the rudimentary successional lamina overhanging the TBI on the lingual side (Figure 2c,c′). At the point of connection between the dentine and bone, the cells on the inside of the tooth had a distinctive elongated shape and were clearly polarized, a feature of odontoblasts (Figure 2b). These cells, and the neighboring odontoblasts and osteoblasts, were RUNX2-positive, along with the dental epithelium (Figure 2d). As RUNX2 can be expressed in both odontoblast- and osteoblast-like cell populations (Jiang et al., 1999), other markers were analyzed to build a picture of the identity of the TBI cells. First, we analyzed ion channel and ion binding proteins, which exhibit differential expression and function in diverse hard-tissue-producing cells. First, we analyzed the presence of

FIGURE 2 Acrodont ankylosis is mediated by a transient odontoblast-like cell population. (a) Micro-CT analysis displays mineralized bone and dentine in different color shades according to its wall thickness. The immediate contact between dentine and bone was established by deposition of tissues as visualized by micro-CT. (a′, a″) Details of dorsal view on the lower jaw visualizing closure of bone lamellae (bl) and only small channels left (arrowheads) between dental pulp and bone marrow. Bone pedicles (bp, arrowheads) extend along the jaw in the lingual and labial area, and bone bridges were also visible in the interdental area (red arrowhead). (b) Before dentine and bone fusion, the dental pedicles elongated, and the shape of both structures was adjusted for contact. (b, b″) Interim tissue is produced by the cluster of elongated polarized cells (ankyloblasts, arrowheads) located near the TBI area. (c′, c″) Pan-cytokeratin labelling highlights the epithelial cells adjacent to TBI's labial part (lacl) (c′, arrowheads). At the lingual side (licl), the epithelium was merging with the successional dental lamina (c″, sdl) and a cluster of polarized cells was located in the TBI area (arrowheads). (d′, d″) RUNX2-positivity of elongated cells (ankyloblasts) indicated their differentiation potential to cells producing mineralized tissue. (e–g′) To visualize the overall morphology and metabolic activity of elongated odontoblast-like cells, the detection of Na,K-ATPase protein expression was performed. (f, f′, g, g′) Besides the positive oral epithelium, the strong Na^+,K^+-ATPase activity was confirmed in odontoblasts and odontoblasts-like cells along the inner periphery of the dental pulp. Note the difference between Na^+,K^+-ATPase expression in odontoblast-like cells/ankyloblasts (arrowheads) and osteoblasts underneath, which lack the Na^+,K^+-ATPase positivity (f, g). Bone pedicle is outlined by dotted line. (h–j′) Calbindin expression shows differences between fully differentiated and active odontoblasts and odontoblast-like cells, producing a transitional mineralized matrix connecting the bone pedicles and dentine (h). (i, i′, j, j′) A clear border between the Calbindin-positive odontoblasts and negative ankyloblasts (arrowheads) is visible in detail. (k–n) Atypically vertically oriented bodies of cells embedded between dentine (d) and bone (b) were observed both at the labial (k—lower power, l—detail) and the lingual side (m—lower power, n—detail) in transmission electron microscope. (o–o″) TRAP-positive cells appeared in dental pulp near the blood vessels and in close proximity to the cluster of ankyloblasts (arrowheads). (p′, p″) CD68-labeled cells displayed same pattern of distribution, where the majority of CD68-positive cells were located near the blood supply and close to ankyloblasts. (q′, q″) TUNEL assay displays the increased number of apoptotic cells within or near the cluster of ankyloblasts. b, bone tissue; bp, bone pedicle; bl, bone lamella; bv, blood vessels; d, dentine; lacl, labial cervical loop; ob, osteoblasts; od, odontoblasts; sdl, successional dental lamina; TBI, tooth–bone interface.

14697580, 2026, 2, Downloaded from https://onlinelibrary.wiley.com/doi/10.1111/joa.70059 by Brno University Of Technology, Wiley Online Library on [31/03/2026]. See the Terms and Conditions (https://onlinelibrary.wiley.com/terms-and-conditions) on Wiley Online Library for rules of use; OA articles are governed by the applicable Creative Commons License

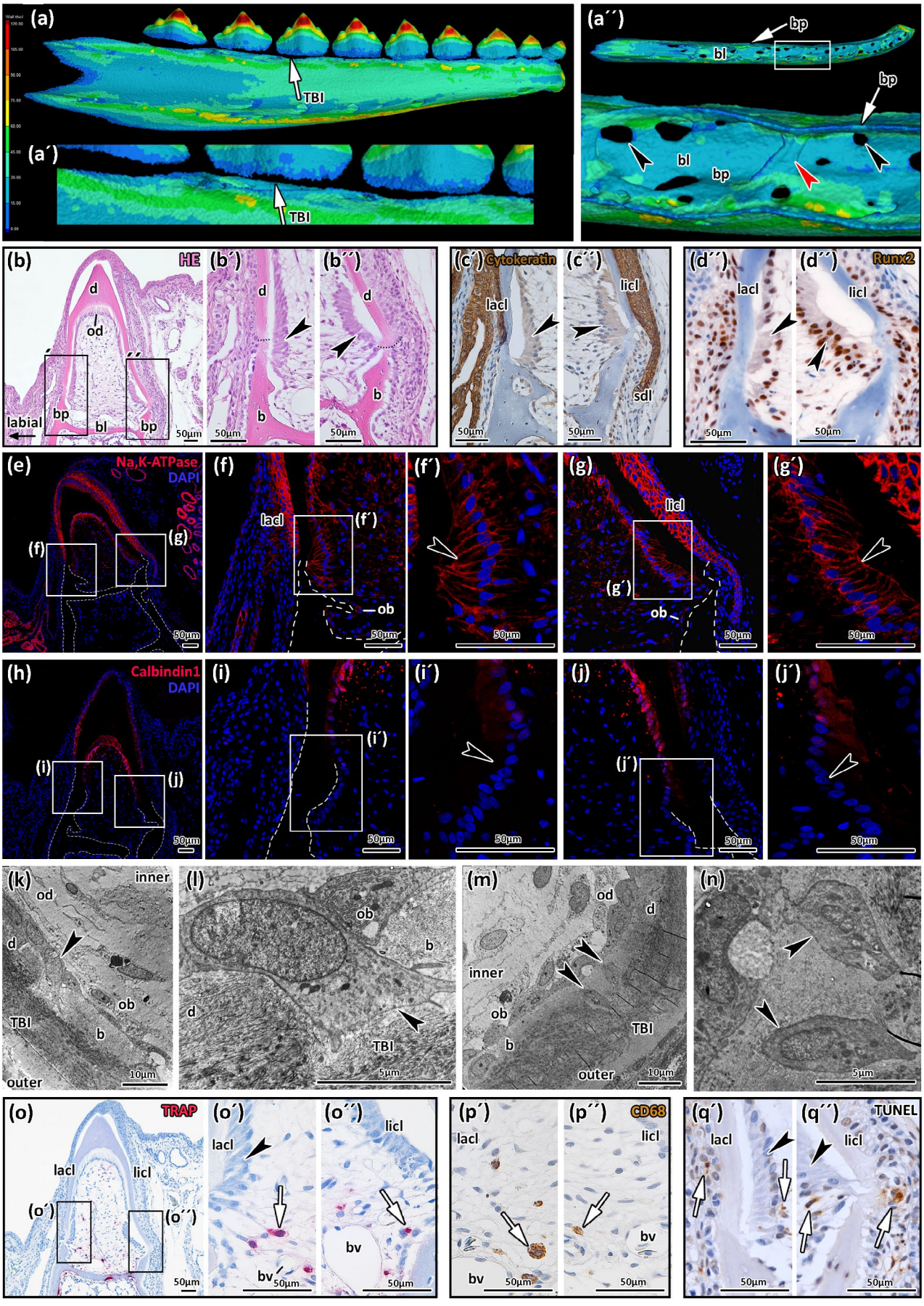

14697580, 2026, 2, Downloaded from https://onlinelibrary.wiley.com/doi/10.1111/joa.70059 by Brno University Of Technology, Wiley Online Library on [31/03/2026]. See the Terms and Conditions (https://onlinelibrary.wiley.com/terms-and-conditions) on Wiley Online Library for rules of use; OA articles are governed by the applicable Creative Commons License

a sodium-potassium ATPase pump that is located in cell membranes and is essential for ion transport (Garcia et al., 2018). Na^+/K^+-ATPase was expressed in membranes of differentiated ameloblasts and odontoblasts and the epithelial cells of the labial and lingual cervical loops, stellate reticulum, and successional dental lamina (Figure 2e–g′). Importantly, osteoblasts only weakly expressed Na^+/K^+-ATPase (Figure 2g). The cluster of elongated cells at the forming TBI exhibited strong Na^+/K^+-ATPase expression, in keeping with an odontoblast-like identity (Figure 2f,f′,g,g′).

To further characterize the population of cells located near the TBI, we analyzed the expression pattern of Calbindin 1 (Vitamin D-dependent calcium-binding protein, Avian-Type) (Berggård et al., 2002) (Figure 2h–j′, Figure S4a–f), which belongs to the group of calcium-binding proteins with distinctive expression in odontoblasts (Kawasaki, 2009; Kawasaki et al., 2021). The Calbindin1 signal was strong in the cytoplasm of differentiated odontoblasts up to the level of the TBI and was absent from the osteoblasts around the bone (Figure 2i,j′). The polarized TBI cells, however, showed no expression of Calbindin1 (Figure 2i,j′, Figure S4e,f), suggesting that they are not typical odontoblasts.

Ultramicroscopic analyses of the dental area uncovered long odontoblast processes embedded in the ECM, while only very thin processes protruded from the osteoblasts at the bony pedicles (Figure S5a–e). The osteoblast bodies ran parallel to the bone surface and contained a large endoplasmic reticulum (Figure 2k). By contrast, the cells producing the TBI exhibited distinct morphologies with several cellular processes protruding toward the matrix, large nuclei, and few organelles (Figure 2l–n). Their bodies were very tall and oriented perpendicularly to the surface (Figure 2l), and this appearance was preserved even after they were embedded in matrix (Figure 2n).

The elongated cells surrounding the TBI area just before fusion, therefore, displayed numerous intermediate characteristics, partly resembling odontoblasts but with some features of osteoblasts and other morphological features unlike osteoblasts or odontoblasts. To distinguish this morphologically and molecularly distinct population, we refer to them as ankyloblasts, reflecting their role in fusion. Interestingly, a similar elongated population of cells at the forming TBI was also observed in other reptiles during tooth attachment, suggesting that these cells play a conserved role (Figure S5).

3.3 | The presence of apoptotic cells in the TBI area suggests a temporary role for ankyloblasts during TBI formation

During the fusion stage, we detected several clusters of TRAP-positive cells adjacent to the emerging ankylosis area on the inner side of the tooth (Figure 2o,o′,o″). In addition, multinucleated osteoclasts were observed predominantly on the bone lamellas surrounding the dental channels, connecting the bone marrow with the dental pulp (Figure 2o, Figure S3i,j). While TRAP stain is commonly used as a marker for bone-resorbing osteoclasts, studies have shown that some macrophage populations, particularly those involved in tissue remodeling or inflammation, may exhibit TRAP activity as well (Oddie et al., 2000). The expression levels in macrophages are typically lower and more variable, and their TRAP activity may not be functionally equivalent to that of osteoclasts (Oddie et al., 2000). To distinguish these two cell types, we evaluated the expression of CD68, a well-known macrophage marker (Holness & Simmons, 1993) (Figure 2p′,p″). A few CD68-positive cells were identified in the dental pulp near the vessels (Figure 2p′,p″), and in several cases, CD68-positive macrophages were located close to clusters of ankyloblasts (Figure 2p′), indicating activation of macrophages in this area. In addition, many of the ankyloblasts in the TBI region were positive for TUNEL, suggesting that at least some of these cells undergo apoptosis and, therefore, represent a transiently active cell population (Figure 2q′,q″, Figure S3s,t).

3.4 | Ankyloblasts cannot be identified after fusion of the tooth and bone

After tooth–bone fusion (Figure 3a,a″), the TBI area further thickened during the late prehatching stages, the "Ankylosis strengthening

FIGURE 3 Ankyloblasts disappear after fusion of the tooth and bone. (a, a′) Once the dentine and bone are connected, the bone lamellae (bl) entirely separates the bone marrow of the jawbone from the dental pulp (a′). Few communicating canals (bc) were present to provide the necessary blood and nerve supply (a″). Note the highest wall thickness in the area just underlying bone pedicles (bp) and the highest thickness in the interdental area (a, red arrow). (b, b′, b″) Pan-cytokeratin labeling did not reveal the presence of elongated ankyloblasts at the inner side of the dental pulp, and epithelium overhangs TBI area. The border between bone and tooth is indicated by a black dashed line. (c, c′) Na^+,K^+-ATPase-positive cells are mostly located in the epithelium. (c′) Flat cells covering the inner side of the dental pulp exhibit only weak Na^+,K^+-ATPase expression. The outlines of the bone are labeled by a white dashed line. (d–d″) Only a few TRAP-positive cells were visible in the dental pulp (d). TRAP-positive cells were found mostly along the inner side of the bone pedicles, where they participate in the constant bone remodeling (d′, d″, arrowhead). (e–e″) Apoptotic cells were sporadically dispersed in the bone as osteocytes trapped in the lacunae of the emerging labial bone pedicle (e′, arrowheads). (f–m) Ultrastructural analyses of TBI area on the lingual side in transmission electron microscope (f—low power picture). (g, h) Cells located at the outer side of the newly formed interface display features of cells with epithelial origin, such as ameloblasts. (i) These cells were in direct contact with the osteoblast cells. (j–m) The inner side of the interface area was covered by the flat cells classified as odontoblasts because of their characteristic appearance of mitochondria (k) and flattened osteoblasts, with very thin processes protruding into the bone matrix (arrowheads) located in deeper areas (m). (l) These two populations were easily recognizable on the border according to their distinct features. am, ameloblast; b, bone; d, dentine; lacl, labial part of the cervical loop; licl, lingual part of cervical loop; ob, osteoblast; od, odontoblasts; sdl, successional dental lamina.

14697580, 2026, 2, Downloaded from https://onlinelibrary.wiley.com/doi/10.1111/joa.70059 by Brno University Of Technology, Wiley Online Library on [31/03/2026]. See the Terms and Conditions (https://onlinelibrary.wiley.com/terms-and-conditions) on Wiley Online Library for rules of use; OA articles are governed by the applicable Creative Commons License

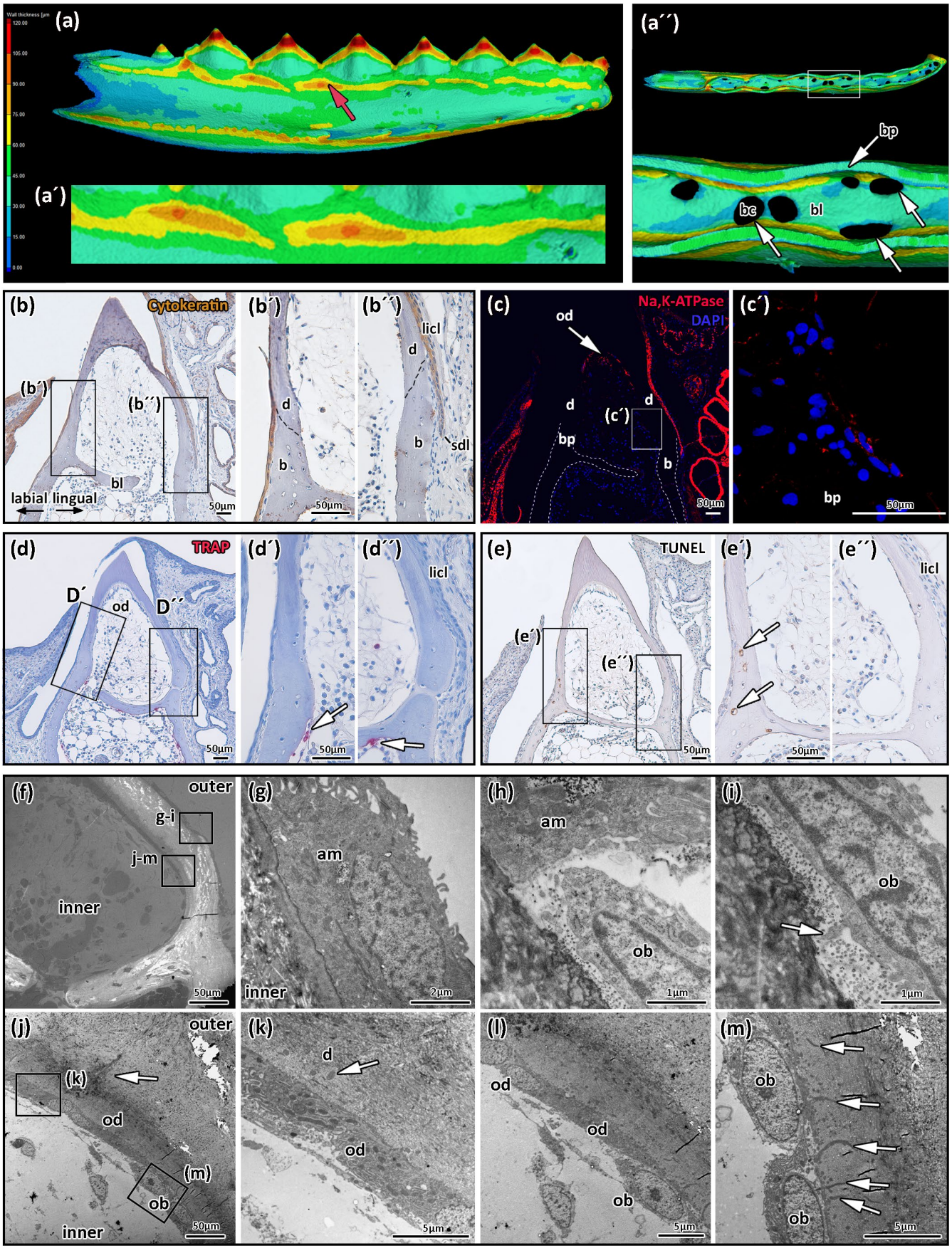

14697580, 2026, 2, Downloaded from https://onlinelibrary.wiley.com/doi/10.1111/joa.70059 by Brno University Of Technology, Wiley Online Library on [31/03/2026]. See the Terms and Conditions (https://onlinelibrary.wiley.com/terms-and-conditions) on Wiley Online Library for rules of use; OA articles are governed by the applicable Creative Commons License

stage" (AS stage—stage 4 of TBI formation), and the merger of both tissues was reinforced (Figure 3b,b″). Analysis of wall thickness revealed thickened areas of bone just under the pedicles and in the areas between the teeth, which are likely to strengthen the tissue exposed to high pressure.

The area of fusion became more difficult to distinguish using histology; however, the bone could be distinguished by the presence of trapped cells, which were not visible in the acellular dentine (Figure 3b). At this stage, the internal part of the TBI was covered by flattened cells (Figure 3c,c′), which is also typical of odontoblasts after they finished secretory activity (Couve et al., 2013). These cells also displayed other substantial differences compared to the elongated odontoblasts located at the tip of the dental pulp (Figure 3d,e). The flattened cells of the TBI area displayed only weak Na^+/K^+-ATPase positivity (Figure 3c,c′), whereas the active and mineralized matrix-producing odontoblasts exhibited a strong Na^+/K^+-ATPase signal at the tip of the dental pulp (Figure 3c). TRAP- and TUNEL-positive cells were no longer associated with the inner surface of the TBI (Figure 3d,d″,e). A few apoptotic cells were identified but restricted to the bone lacunae (Figure 3e,e″), which is expected as some osteocytes would be removed during this period.

Using TEM, fully differentiated cells (osteoblasts, odontoblasts, and ameloblasts) were located on the surface of the bone and dentine (Figure 3f–m, Figure S6a–h). Ameloblasts with discontinuous basal lamina ended sharply at the TBI zone on the outer side of the tooth germ (Figure 3g,h). The presence of organelles, the appearance of the cytoplasm, and processes were used to clearly identify osteoblast versus odontoblast cells in the TBI zone (Figure 3k,m). While osteoblasts had multiple thin processes extending from the cell body (Figure 3m); odontoblasts had a single primary process (Tomes' fiber) protruding from the cell body (Figure S6a,b). This primary protrusion branched as it penetrated the dentine matrix (Figure S6c,d). A layer of typical osteoblasts was evident from the TBI to the bone pedicle (Figure 3h,i). On the inner side of each tooth germ facing the dental papilla (Figure 3j–m), an exact border between odontoblasts and osteoblasts was not evident when viewed under a light microscope. However, electron micrographs revealed a boundary between these cells at the TBI (Figure 3l). Osteoblasts with enlarged endoplasmic reticulum were located deeply in the TBI toward the bone, with a few osteoblasts overlapping the dentine area on the inner surface of the TBI facing the dental papilla (Figure 3l,m).

In summary, the TBI cells were flattened with many elongated mitochondria displaying some odontoblastic features, and osteoblasts were observed covering these cells. Tall TBI cells (ankyloblasts), observed at the stage before tooth–bone fusion, were no longer apparent after fusion by histology or by TEM.

3.5 | The TBI extracellular matrix exhibits distinct features even after tooth–bone fusion

Next, we asked if there were differences in the structure of the tooth attachment tissue and dentine/bone ECM tissues. This could further support a distinct origin of the tooth attachment tissue and confirm which cell type contributed to its production. We used TEM at a later developmental stage to assess the features of the TBI hard tissues in the older stage when attachment was already formed (Figure 4a–d, Figure S7a–d). Dentine and bone tissues in the chameleon demonstrated many common features similar to those of other animals (Figure 4b, Figure S7a–d). The difference between dentine and bone was based on the thickness of the cytoplasmic cellular processes embedded within the ECM. Moreover, the collagen fibrils surrounding the osteoblasts were characteristically arranged in a regular, unidirectional pattern beneath the osteoblasts, in contrast to more irregularly arranged fibrils observed adjacent to the odontoblasts (compare Figure 4d and Figure S7c,d).

The tooth–bone interface displayed an uneven arrangement with the transitional zone located more deeply on the inner side facing the dental papilla. At the same time, on the outer side, the dentine–bone interface was nested rather superficially toward the oral cavity. Electron-dense extracellular matrix localized beneath the cell (Figure 4b,d) exhibited the strongest mineralization at the

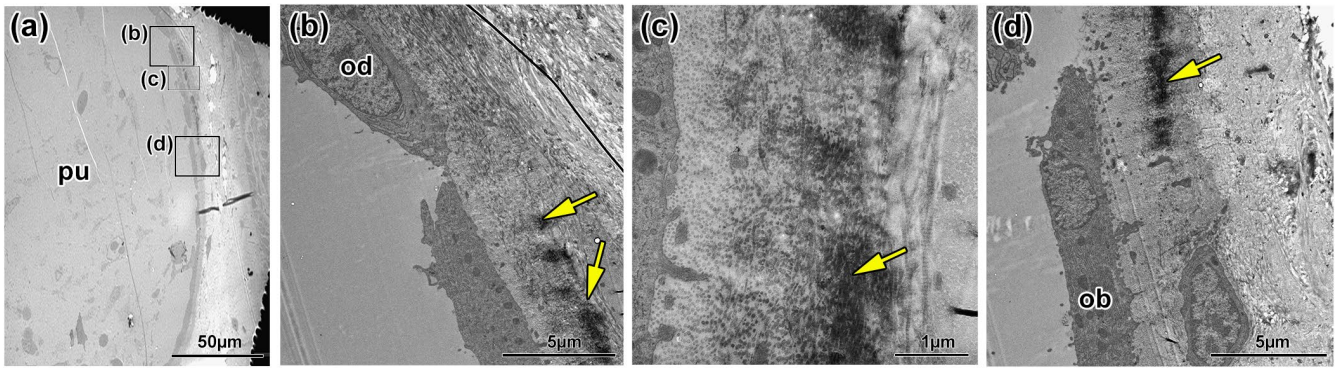

FIGURE 4 TEM of the tooth–bone interface after tissue fusion. (a) Low power magnification of the tooth–bone interface in animal after full fusion of bone and tooth. (b) The border between odontoblast area (od) and TBI region (yellow arrow). Collagen fibrils are arranged irregularly in the dentine area. (c) Mineralization of extracellular matrix is increased in the TBI area (yellow arrow) with the deeper layers irregularly organized collagen fibres. (d) The border between TBI region (yellow arrow) and bone with osteoblasts (ob).

14697580, 2026, 2, Downloaded from https://onlinelibrary.wiley.com/doi/10.1111/joa.70059 by Brno University Of Technology, Wiley Online Library on [31/03/2026]. See the Terms and Conditions (https://onlinelibrary.wiley.com/terms-and-conditions) on Wiley Online Library for rules of use; OA articles are governed by the applicable Creative Commons License

tooth–bone interface (Figure 4c) with a distinct appearance compared to the neighboring bone and dentine matrix. In the TBI, collagen fibrils were arranged partly in a regular, bone-like pattern in the superficial layer, but irregularly in the deeper layers; this fibrillar organization was not observed in other regions of the bone pedicle or dentine (Figure 4c, Figure S7c).

In conclusion, the extracellular matrix connecting the dentine and bone pedicles demonstrated distinct features, including higher mineralization and mixed features of organization of collagen fibrils.

3.6 | Late-stage maturation of the tooth–bone interface in juvenile chameleons

At a posthatching stage (2-month-old juveniles), the "Maturated ankyloses stage" (MA stage—stage 5 of TBI formation), we observed broadening of the hard tissues, indicating a continuation of hard-tissue deposition in juvenile animals (Figure 5a,a″). The dentine–bone boundary was progressively bridged by a mineralized extracellular matrix (Figure S8a,b). This physically inseparable border displayed distinct layers of dentine and bone overlaying each other, indicating a nonuniform deposition of these two components (Figure 5b,b″). TRAP-positive cells appeared dispersed within this zone, indicating constant rearrangement of mineralized tissues in the TBI area (Figure 5b′,b″).

To determine the hard matrix allocation dynamics in the TBI and especially the formation of distinct hard-tissue layers, we injected Calcein Green and Alizarin Red into juvenile chameleon animals (Figure 5c–g, Figure S8a–k). These fluorescent dyes can be incorporated into forming mineralized tissue by binding to calcium ions during mineralization. Therefore, they can serve as a tool for evaluating the process of bone or dentine deposition (Pautke et al., 2005, 2007). Two different intervals were selected for the injection of the dyes: 3- and 6-day intervals (Figure 5c–g, Figure S8).

The most distinct signal was located on the tip of the tooth, indicating that odontoblasts were still actively contributing to the process of dental pulp filling even after tooth eruption (Figure 5d,e, Figure S8a,e). The fluorescent signal appeared distributed along the labial and lingual surfaces of the dental pulp, confirming the activity of odontoblasts at the lateral areas of the tooth and their contribution to dental pulp filling (Figure 5f–g, Figure S8a–c,e–h). As expected, we did not find any Calcein Green or Alizarin Red dyes incorporated in the tooth's enamel layer, the ameloblasts having been lost earlier during tooth eruption (Figure 5f–g, Figure S8a–h).

The signal for both dyes appeared distinct at the surface of the inner and outer sides of the bone pedicles (Figure S8a,c,e,g). The Alizarin Red signal was also evident on the superficial layer of the bone lamella underlying the tooth on the side facing the dental pulp, indicating filling of the dental pulp by osteoblasts from the bottom of the tooth (Figure S8a,c). At both selected time intervals, the pattern of hard-tissue deposition was similar (Figure S8a–d,e–h).

In the TBI area, we detected weak Calcein Green and Alizarin Red signals (Figure 5f–g, Figure S8a,d,e–h) in contrast to the interdental area and underlying bony lamellae, where the signal was strong (Figure 5h–j). Interestingly, on the lingual side of the TBI, the Calcein Green and Alizarin Red signals were stronger along the outer side of the jawbone as well as at locations adjacent to the dentine. This suggests higher osteoblast activity on the lingual side (Figure 5g, Figure S8d,h) in contrast to the labial side (Figure 5f), where no similar activity was detected in either selected interval. This finding confirmed the previously observed morphological differences between the labial and lingual sides observed at earlier stages (Figure 3b,b′,b″), where the labial part becomes almost naked during development while the lingual part is well covered by soft tissues.

The cells located at the TBI zone displayed very weak Na^+/K^+-ATPase and Calbindin1 expression (typically marking flattened osteoblasts) (Figure 5k–l′). By contrast, the metabolically active odontoblasts under the tip of the tooth demonstrated overlapping and strong expression of Na^+/K^+-ATPase and Calbindin1 (Figure 5k′,l′). These findings support the observation that osteoblasts superimpose the dentin produced in the early stages, and the bone matrix overlaps the region of TBI during the posthatching stages.

4 | DISCUSSION

Differences in the arrangement of the tooth–bone interface have previously been described in several extant and extinct vertebrates (Budney et al., 2006; Caldwell, 2007; Caldwell et al., 2003; Luan et al., 2009; Rieppel & Kearney, 2005; Zaher & Rieppel, 1999). Despite the significant number of studies focusing on this topic, how non-thecodont attachment tissue is produced during development and by which cell types remains unclear. Thus, our study aimed to identify the cell types contributing to the formation of acrodont ankyloses and to characterize the molecular features of the cells and the nature of the attachment tissue they produce. To this end, we divided the attachment period into five stages (Figure 6): (1) Initiation of interface formation stage - the early stage, when the tooth and bone are at a distance however group of mesenchymal cells was spanning the gap between tooth and bone; (2) Hard-tissue rearrangement stage - when the dental and bone tissues start to interact; typical by rearrangement of dental tissue and bone pedicle formation; (3) Attachment tissue production stage with close interaction between the tooth and bone including the mineralization of the tooth attachment matrix; (4) Ankylosis strengthening stage with thickening of the tooth–bone interface area and finely by consolidating the connection during its maturation stage (5).

4.1 | RUNX2 marks early tooth–bone interface cells with the potential for mineralized tissue production

To determine the characteristics of cells contributing to TBI, we followed RUNX2, one of the transcription factors previously described as important for the differentiation of cells producing hard

14697580, 2026, 2, Downloaded from https://onlinelibrary.wiley.com/doi/10.1111/joa.70059 by Brno University Of Technology, Wiley Online Library on [31/03/2026]. See the Terms and Conditions (https://onlinelibrary.wiley.com/terms-and-conditions) on Wiley Online Library for rules of use; OA articles are governed by the applicable Creative Commons License

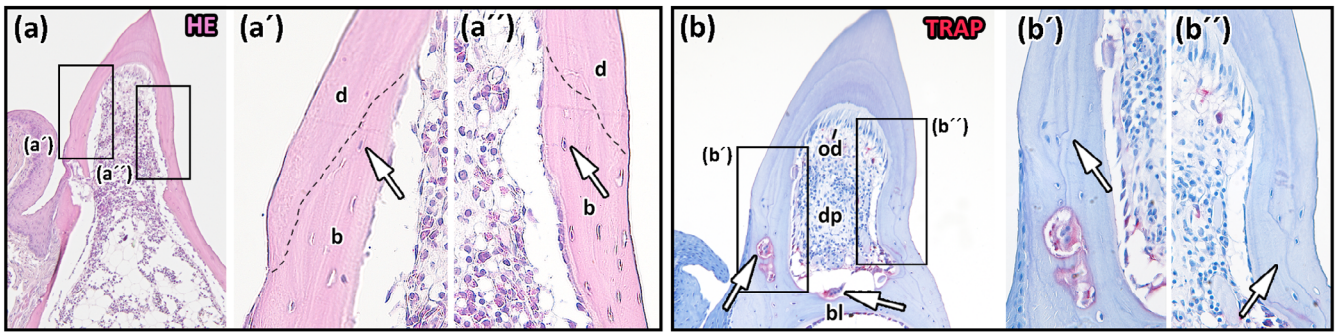

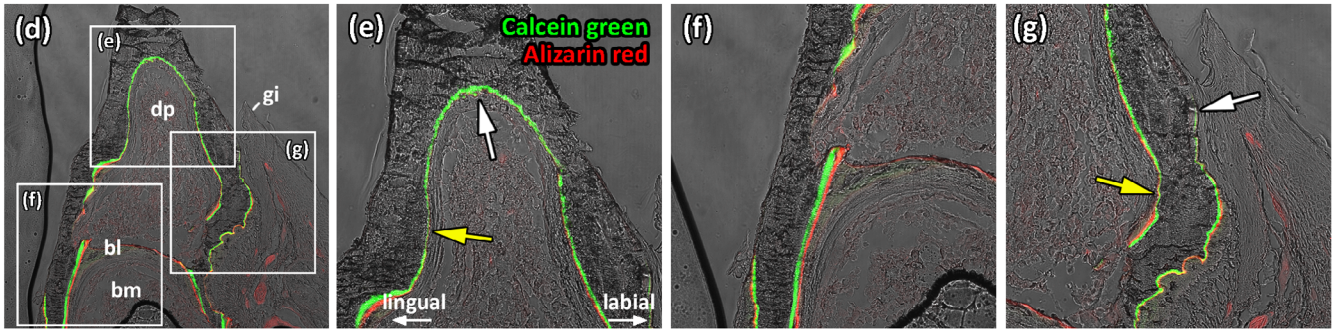

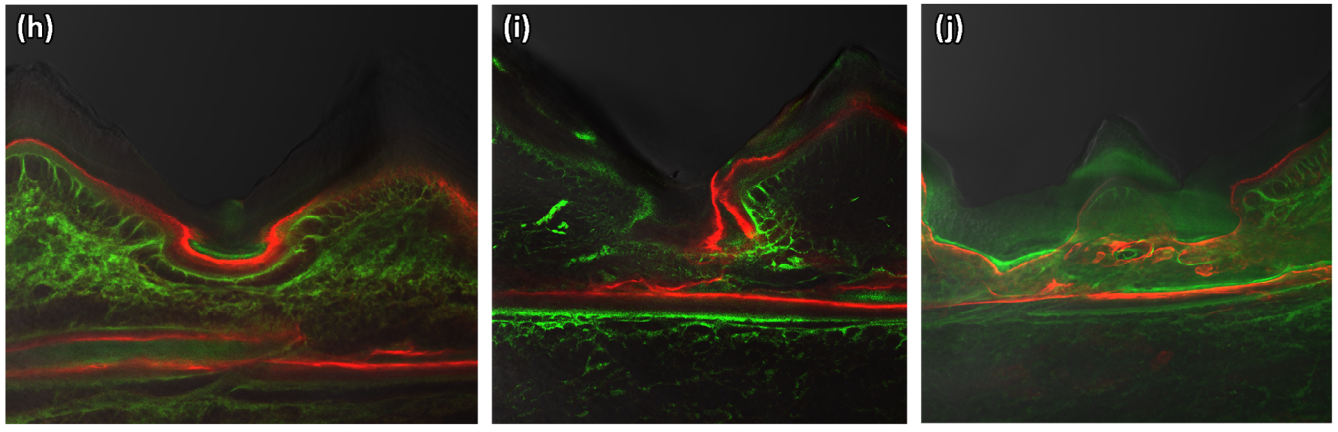

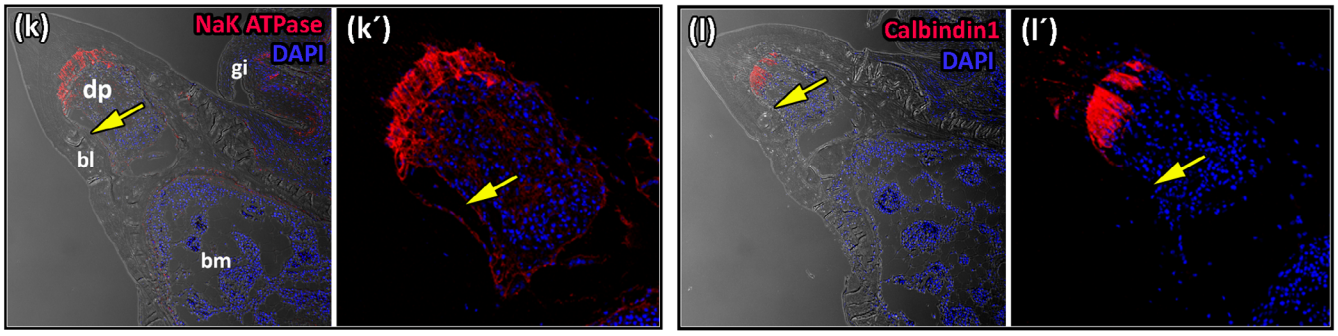

14697580, 2026, 2, Downloaded from https://onlinelibrary.wiley.com/doi/10.1111/joa.70059 by Brno University Of Technology, Wiley Online Library on [31/03/2026]. See the Terms and Conditions (https://onlinelibrary.wiley.com/terms-and-conditions) on Wiley Online Library for rules of use; OA articles are governed by the applicable Creative Commons License

FIGURE 5 The TBI area is expanded by strengthening bone mass around the dentine by osteoblasts during posthatching odontogenesis. (a–a″) At the juvenile stages, the bone and dentine were firmly fused to form one inseparable entity with the osteocyte-containing lacunae covering the base of the teeth as visualized by Hematoxylin–Eosin staining (a–a″, arrowheads). (a′, a″) The border between the dentine and bone, indicated here by the black dashed line, was less visible during the posthatching stages. (b–b″) Individual mineralized tissue layers can be visualized (arrowheads). (b) The elongated odontoblasts were still present at the tip of the dental pulp where dentine was deposited, while the TBI area was covered by flat cells (b′, b″). The TRAP-positive cells (red cells) were located mostly along the emerging bone lamellae and inside the lacunae of the jawbone or dental papilla. (c–j) Vital dyes were used to visualize the dynamics of hard tissue deposition in the TBI area as they naturally incorporate into the newly deposited mineralized tissue. (c) Calcein Green and Alizarin Red dyes were injected at 6-day intervals. (d–g) Mineralization occurs along the inner walls of the dental pulp and along both the inner and outer sides of the jawbone, as visualized on transversal sections. (e) Vital dyes were incorporated in the dentine matrix (d) adjacent to differentiated odontoblasts. (f) In the labial side, the matrix was deposited preferentially from the dental pulp (TBI area labeled by yellow arrow). On the outer side, there was production visible just in deeper areas, which was in agreement with oral epithelium remission in this area in juvenile animals. (g) On the lingual side, the production of matrix occurred both at the inner and outer surfaces. In contrast to the labial side, the bone matrix newly deposited by osteoblasts extends superficially (white arrowhead) and overlaps TBI (yellow arrow) at the tooth's outer surface. (h–j) Whole mount visualization of Calcein Green and Alizarin Red-labeled animals display deposition of hard tissues in the interdental area (ida) and TBI area (yellow arrowhead) as well as along underlying bone lamellae (bl). (k, k′) The strongest Na^+,K^+-ATPase positivity was manifested mostly in odontoblasts (od). The TBI area (yellow arrowhead) exhibited only weak Na^+,K^+-ATPase signals. (l) Similarly, odontoblasts also strongly express Calbindin (l′), while the TBI area (yellow arrowhead) exhibited no calbindin positivity (l′). b, bone; bl, bone lamellae; bm, bone marrow; bp, bone pedicle; d, dentine; dp, dental pulp; gi, gingiva; ida, interdental area; od, odontoblasts.

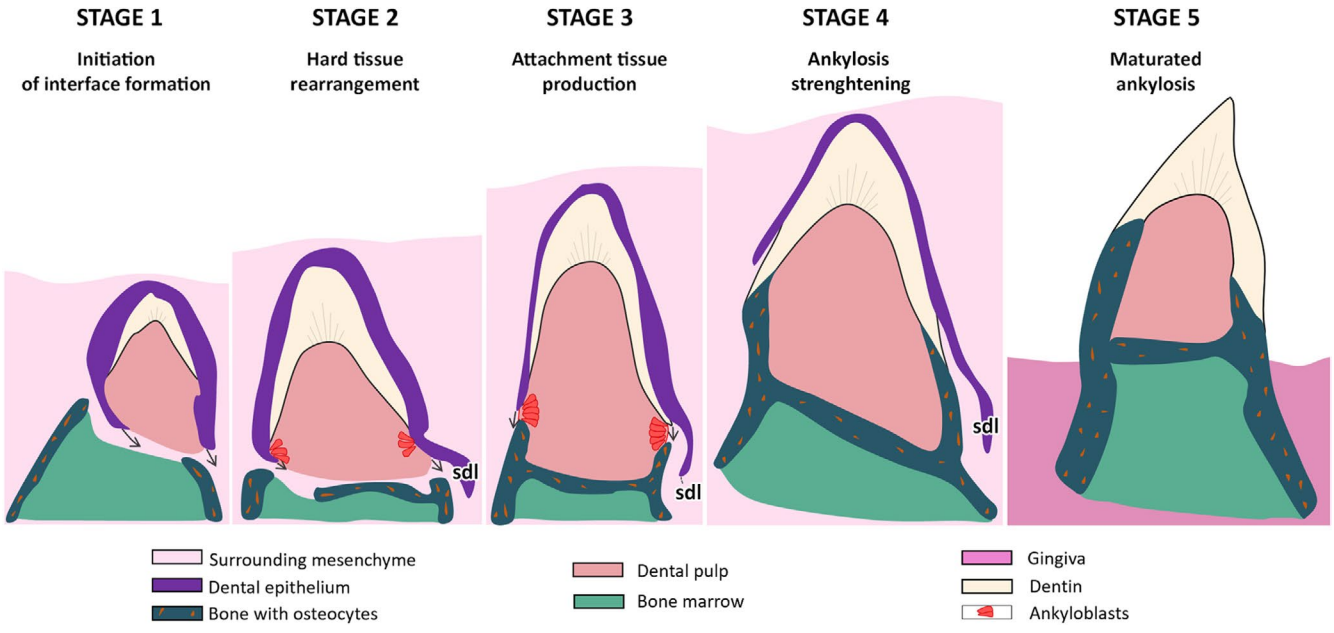

FIGURE 6 Schematic representation of ankylosis development.

tissues while also controlling their proliferation and maintenance (Camilleri & McDonald, 2006). RUNX2 is primarily known for its role in osteoblast differentiation and skeletal development, but it also plays roles in epithelial–mesenchymal interactions during craniofacial and tooth development. Previous studies have shown that developing epithelium, including dental epithelium such as ameloblasts and cells of the cervical loop, can express RUNX2 (Camilleri & McDonald, 2006; D'Souza et al., 1999). This expression often occurs transiently and is involved in regulating signaling pathways that influence mesenchymal cell fate. Other studies have also observed RUNX2 in proliferative regions of the oral epithelium, even in nontooth-bearing areas (Tan et al., 2017). Consistent with this, we also observed RUNX2 expression in the inner enamel epithelium of chameleons, similar to findings in mice where RUNX2 is expressed in ectodermally derived ameloblasts during the maturation phase of enamel formation (D'Souza et al., 1999; Jiang et al., 1999).

Moreover, *Runx2* is upregulated in mouse preodontoblasts (Liu et al., 2005) and later downregulated in differentiated odontoblasts. Similar to the situation in the mouse (D'Souza et al., 1999), RUNX2 was expressed in the mesenchyme of the chameleon dental papilla and in all osteoblasts and osteocytes. As the odontoblasts became fully differentiated, RUNX2 expression became weaker, similar to that previously described in mammalian model species (Bertonnier-Brouty et al., 2021; Wu et al., 2020).

RUNX2 can contribute to maintaining the periodontal ligament in mammals through regulation of osteogenesis in this area (Camilleri & McDonald, 2006; Komori et al., 1997; Otto et al., 1997). In chameleons, the cells linking the tooth and the bone formed a

14697580, 2026, 2, Downloaded from https://onlinelibrary.wiley.com/doi/10.1111/joa.70059 by Brno University Of Technology, Wiley Online Library on [31/03/2026]. See the Terms and Conditions (https://onlinelibrary.wiley.com/terms-and-conditions) on Wiley Online Library for rules of use; OA articles are governed by the applicable Creative Commons License

RUNX2-positive collar, suggesting that the identity of the TBI was already established at these early stages and that these cells had the potential to differentiate into cells contributing to hard tissue production.

4.2 | An intermediate cell type at the tooth–bone interface

When we evaluated chameleon embryos from different developmental stages just prior to the connection of the tooth and bone, a morphologically distinct population of cells was evident in the TBI area. These cells, located around the end of the cervical loop, were elongated and distinct from the neighboring odontoblasts and osteoblasts. The position and continuity with the odontoblast layer suggest they may represent an intermediate stage in the differentiation pathway, specifically adapted to support mineralized tissue deposition at this critical junction. In keeping with this, these elongated cells exhibited odontoblast-like properties at the ultrastructural level and expressed high levels of Na^+/K^+-ATPase, which was also detected in odontoblasts located at the tip of the tooth. In contrast, the adjacent osteoblasts located along the bone lamella and pedicles exhibited weak expression of Na^+/K^+-ATPase scattered unevenly along their cell membranes. However, like osteoclasts, the TBI cells did not express Calbindin1, which is highly expressed in odontoblasts, suggesting that the TBI cells were distinct from mature odontoblasts. Interestingly, the Calbindin1 expression in chameleon remained only in the tooth tip area and did not expand further even after the tooth/dentine contacted the jawbone. A similar expression pattern restricted to the tip of the dental papilla was observed for some calcium-binding proteins in zebrafish (Rosa et al., 2021). Therefore, Calbindin1 may label only a specific subpopulation of odontoblasts (Kawasaki, 2009).

Based on their distinct morphology, localization, and molecular profile, we have termed these TBI cells "ankyloblasts" to describe a transient cell population observed during the formation of dental ankyloses. Here the term "ankyloblast" is intended as a descriptive label rather than a designation of a fundamentally novel skeletal cell type. These cells represent odontoblast-like cells in a temporally restricted and active secretory phase specific to the process of ankylosis initiation. Similar elongated cells lining the future or forming TBI region were also observed in other reptile species prior to ankyloses and have previously been observed in snakes (LeBlanc et al., 2023) and even in catfish, where odontoblast-like cells were observed between the dentine and the attachment bone attached to both matrices by cellular processes (Huysseune & Sire, 1997). This transient cell type might, therefore, be conserved.

The disappearance or flattening of these TBI cells coincided with the presence of TUNEL-positive cells and macrophages, suggesting that this population might undergo apoptosis and/or be removed by phagocytosis.

The TBI-associated cells exemplify a broader biological principle observed across vertebrate skeletal systems: the plasticity and functional overlap among mesenchymal-derived cell types involved in mineralized tissue formation. Rather than representing an exception, these cells highlight the continuum between osteogenic and odontogenic phenotypes, a concept well established in developmental and evolutionary biology. Similar transitional or hybrid cell states have been reported in various contexts, including the formation of osteodentine, cementum, and bone of attachment. The morphological and molecular features of the TBI-associated cells, while distinctive in their spatial and temporal context, are consistent with the known capacity of skeletal cells to adopt intermediate identities in response to local signals and functional demands (Beresford, 1981; Cole & Hall, 2004; Hallett et al., 2021; Kodama et al., 2022; Zhu et al., 2024). As such, these cells should be viewed as part of this dynamic spectrum, offering further insight into the mechanisms by which vertebrates generate structurally diverse mineralized interfaces.

4.3 | The character of the matrix of the tooth–bone interface

The origin of tissue at the tooth–bone interface has been a topic of extensive discussion for many years, most often studied in the context of pleurodont implantation and tissue, where this tissue connects the tooth and bone on the labial side (Westergaard & Ferguson, 1986, 1987). The junction between the tooth base and the bone has been described to be formed by cementum, bone, or composed of mineralized periodontal ligaments, creating different types of "bone of attachment" (Dosedělová et al., 2016; LeBlanc et al., 2021; LeBlanc, Brink, et al., 2017; LeBlanc, Lamoureux, & Caldwell, 2017; Zaher & Rieppel, 1999). We observed a distinct arrangement of extracellular matrix components in the TBI area, suggesting that this matrix does not originate directly from osteoblasts or odontoblasts. In particular, we noted a difference in density of the mineralized attachment tissue compared to the jawbone, which was already evident from Hematoxylin–Eosin staining. We, therefore, conclude that the ankylosis-associated cells were able to produce a matrix distinct from that produced by osteoblasts and odontoblasts and that this early matrix was the first to unite the tooth and bone.

4.4 | Remodeling of bone tissue for precise ankylosis

The development of the tooth–bone interface in the chameleon was a precisely coordinated process, allowing the shape of the tooth base to match that of the bone pedicle. In the early stages, the tooth germ and the bone pedicles displayed different morphologies; however, remodeling of the bone tissue was evident from the osteoclasts. Interestingly, we found only a few osteoclasts at the tooth–bone interface. The presence of TRAP-positive cells is usually associated with several processes during odontogenesis, including the control of osteoclast activity for regulating the distance between the forming

14697580, 2026, 2, Downloaded from https://onlinelibrary.wiley.com/doi/10.1111/joa.70059 by Brno University Of Technology, Wiley Online Library on [31/03/2026]. See the Terms and Conditions (https://onlinelibrary.wiley.com/terms-and-conditions) on Wiley Online Library for rules of use; OA articles are governed by the applicable Creative Commons License

alveolar bone and the developing tooth germ in mice or odontoclast activity during root resorption prior to the shedding of human deciduous teeth (Alfaqeeh et al., 2013; Handrigan et al., 2010; Handrigan & Richman, 2010; Sahara et al., 1998). In the mouse, the approach of the outer enamel epithelium toward the bone triggers the recruitment of osteoclasts, which act to prevent the dental epithelium and bone from coming too close (Alfaqeeh et al., 2013). This osteoclastic activity is essential to maintain a minimal separation between the two structures and thereby prevent tooth–bone fusion and the initiation of ankylosis (Alfaqeeh et al., 2013). In contrast, reptilian teeth and bones need to join together to form pleurodont or acrodont dentitions, so similar recruitment of osteoclasts or odontoclasts at these stages would be detrimental. Although the chameleon is monophyodont, with no tooth replacement, most lizards and snakes are polyphyodont, with constant tooth replacement. For these species, clast cells play a significant role in physiological tooth resorption allowing shedding of older tooth generations throughout an animal's life (Handrigan et al., 2010; Handrigan & Richman, 2010; Henriquez et al., 2025; Sahara et al., 1998). Numerous osteoclast and odontoclast cells have been observed associated with the teeth of the scincid lizard (Chalcides viridanus), and odontoclasts were also found in the tree iguana *Liolaemus gravenhorsti* (Delgado et al., 2005; Fuenzalida et al., 1999). In the scincid lizard, the difference between the osteoclast and the odontoclast was based on the nature of the tissue they resorbed (Delgado et al., 2005).

In chameleons, only a few TRAP-positive cells were observed at the TBI during the early stages when the two tissues were getting close to each other. However, once the bone and dentine had fused, these cells were observed clustered around the developing bone lamella. TRAP-positive cells in the chameleon thus are likely to be important for the precise control of acrodont implantation, sculpting the bony pedicles as they meet the dentin. In addition to large multinucleated TRAP-positive cells, a few mononucleated TRAP-positive cells were evident in the dental pulp, which in other reptiles have been shown to be capable of becoming multinucleated odontoclasts (LeBlanc et al., 2023; Sahara et al., 1998). Not all mononucleated cells in resorptive zones represent precursors, since mononucleated odontoclasts have also been identified as functional resorptive cells in humans (Domon et al., 1994).

4.5 | Hard-tissue deposition as a dynamic process exhibiting asymmetric features

To determine the dynamics of TBI formation and its rearrangement during posthatching stages when animals could process food, we injected two fluorescent dyes, Calcein Green and Alizarin Red, into 2-month-old chameleons. Both dyes were distinctly visible along the inner side of the dental pulp, as well as in jawbones, indicating intense hard-tissue deposition mediated by osteoblasts and odontoblasts at both analyzed time points. Interestingly, there was a significant increase in bone deposition from the outer side in the lingual area, which led to overgrowth of the TBI area. This indicated that the tooth–bone attachment was hardened by bone tissue, which was already proposed previously based on the microscopic analyses (Dosedělová et al., 2016). Moreover, such a phenomenon closely resembles the subthecodont dentition, where the jawbone forms a shallow socket that covers the dentine body of the tooth from the outside (Bertin et al., 2018). However, in the chameleon, it appears that the bone does not form a proper socket-like structure but rather is produced following elongation of the bone pedicles after the tooth–bone fusion and not before this process, as was described for subthecodont dentitions (Bertin et al., 2018). Our results also confirm both bone and dentine as the origin of the tissues filling the dental pulp, with the odontoblasts actively producing dentine along the entire dental pulp while the bone extends upward from bony protrusions to the pulp from the underlying lamella.

5 | CONCLUSION

In summary, our study has revealed the existence of a transient cell population, the ankyloblasts, which produce the matrix to link the tooth and bone during the formation of an acrodont attachment. Ankyloblasts had distinct morphologies, with elongated shapes, and expressed some but not all odontoblast markers, suggesting they are more similar to odontoblasts than to osteoblasts. Ankyloblasts were evident during the initial fusion of the tooth and bone but then were removed by apoptosis and phagocytosis. After fusion, the connection between the tooth and bone was reinforced by the activity of neighboring odontoblasts and osteoblasts. The ankyloblast population does not seem to be unique to animals with an acrodont attachment, and further analysis will be necessary to understand their occurrence outside this group of reptiles.

AUTHOR CONTRIBUTIONS

Conceptualization: MB, AST; Methodology: MŠ, JD, MK, OZ, VP; Formal analysis: MŠ, JD, MK, OZ; Investigation: MŠ, JD, MK, BH, OZ; Resources: MB, TZ, JKa; Writing—Original Draft: MŠ, JD, MK, OZ, JKr; Writing—Review and Editing: MB, IA, JKr, BH, AST, TZ; Visualization: MŠ, JD, MK, BH, OZ; Supervision: MB, TZ; Funding acquisition: MB, JKa.

ACKNOWLEDGEMENTS

This study was supported by the Czech Science Foundation (22-02794S), and preliminary data were obtained with the support of the Ministry of Health, Czech Republic (NW24-10-00204). This work was financially supported by projects OP RDE, MEYS (Reg. No. CZ.02.1.01/0.0/0.0/16_019/0000728; CZ.02.01.01/00/22_008/0004593, CZ.02.1.01/0.0/0.0/15_003/0000460). We acknowledge the core facility CELLIM supported by the Czech-BioImaging large RI project (LM2023050 funded by MEYS CR) for their support with obtaining scientific data presented in this paper. The authors would like to thank Naděžda Vaškovičová for help with processing semithin and ultrathin sections. Open access publishing facilitated by Ustav zivocisne fyziologie a genetiky

14697580, 2026, 2, Downloaded from https://onlinelibrary.wiley.com/doi/10.1111/joa.70059 by Brno University Of Technology, Wiley Online Library on [31/03/2026]. See the Terms and Conditions (https://onlinelibrary.wiley.com/terms-and-conditions) on Wiley Online Library for rules of use; OA articles are governed by the applicable Creative Commons License

Akademie ved Ceske republiky, as part of the Wiley - CzechELib agreement.

CONFLICT OF INTEREST STATEMENT

The authors declare no conflict of interest.

DATA AVAILABILITY STATEMENT

All data are provided in the manuscript or supplementary material.

ORCID

A. S. Tucker https://orcid.org/0000-0001-8871-6094

REFERENCES

Alfaqeeh, S.A., Gaete, M. & Tucker, A.S. (2013) Interactions of the tooth and bone during development. *Journal of Dental Research*, 92, 1129–1135. Available from: https://doi.org/10.1177/0022034513510321

Beresford, W.A. (1981) *Chondroid bone, secondary cartilage, and metaplasia*. Baltimore: Urban & Schwarzenberg.

Berggård, T., Miron, S., Önnerfjord, P., Thulin, E., Akerfeldt, K.S., Enghild, J.J. et al. (2002) Calbindin D28k exhibits properties characteristic of a Ca^{2+} sensor. *Journal of Biological Chemistry*, 277, 16662–16672. Available from: https://doi.org/10.1074/jbc.M200415200

Bertin, T.J.C., Thivichon-Prince, B., LeBlanc, A.R.H., Caldwell, M.W. & Viriot, L. (2018) Current perspectives on tooth implantation, attachment, and replacement in amniota. *Frontiers in Physiology*, 9, 1630. Available from: https://doi.org/10.3389/fphys.2018.01630

Bertonnier-Brouty, L., Viriot, L., Joly, T. & Charles, C. (2021) Gene expression patterns associated with dental replacement in the rabbit, a new model for the mammalian dental replacement mechanisms. *Developmental Dynamics*, 250, 1494–1504. Available from: https://doi.org/10.1002/dvdy.335

Buchtová, M., Zahradníček, O., Balková, S. & Tucker, A.S. (2013) Odontogenesis in the veiled chameleon (*Chamaeleo calyptratus*). *Archives of Oral Biology*, 58, 118–133. Available from: https://doi.org/10.1016/j.archoralbio.2012.10.019

Budney, L.A., Caldwell, M.W. & Albino, A. (2006) Tooth socket histology in the cretaceous Snake Dinilysia, with a review of amniote dental attachment tissues. *Journal of Vertebrate Paleontology*, 26(1), 138–145.

Caldwell, M.W. (2007) Ontogeny, anatomy and attachment of the dentition in mosasaurs (Mosasauridae: Squamata). *Zoological Journal of the Linnean Society*, 149, 687–700.

Caldwell, M.W., Budney, L.A., Lamoureux, D.O., Caldwell, M.W., Budneyl, L.A. & Lamoureux2, D.O. (2003) Histology of tooth attachment tissues in the late cretaceous Mosasaurid Platecarpus. *Source: Journal of Vertebrate Paleontology*, 23(3), 622–630. Available from: https://doi.org/10.1671/0272-4634(2003)023

Camilleri, S. & McDonald, F. (2006) Runx2 and dental development. *European Journal of Oral Sciences*, 114, 361–373. Available from: https://doi.org/10.1111/j.1600-0722.2006.00399.x

Cole, A.G. & Hall, B.K. (2004) The nature and significance of invertebrate cartilages revisited: distribution and histology of cartilage and cartilage-like tissues within the Metazoa. *Zoology*, 107, 261–273. Available from: https://doi.org/10.1016/j.zool.2004.05.001

Couve, E., Osorio, R. & Schmachtenberg, O. (2013) The amazing odontoblast: activity, autophagy, and aging. *Journal of Dental Research*, 92(9), 765–772. Available from: https://doi.org/10.1177/0022034513495874

Delgado, S., Davit-Beal, T., Allizard, F. & Sire, J.-Y. (2005) Tooth development in a scincid lizard, *Chalcides viridanus* (Squamata), with particular attention to enamel formation. *Cell and Tissue Research*, 319, 71–89. Available from: https://doi.org/10.1007/s00441-004-0950-2

Diekwisch, T.G.H. (2001) Developmental biology of cementum. *The International Journal of Developmental Biology*, 45(5–6), 695–706.

Domon, T., Sugaya, K., Yawaka, Y., Osanai, M., Hanaizumi, Y., Takahashi, S. et al. (1994) Electron microscopic and histochemical studies of the mononuclear odontoclast of the human. *The Anatomical Record*, 240, 42–51. Available from: https://doi.org/10.1002/ar.1092400105

Dosedělová, H., Štěpánková, K., Zikmund, T., Lesot, H., Kaiser, J., Novotný, K. et al. (2016) Age-related changes in the tooth–bone interface area of acrodont dentition in the chameleon. *Journal of Anatomy*, 229, 356–368. Available from: https://doi.org/10.1111/joa.12490

D'Souza, R.N., Åberg, T., Gaikwad, J., Cavender, A., Owen, M., Karsenty, G. et al. (1999) Cbfa1 is required for epithelial-mesenchymal interactions regulating tooth development in mice. *Development (Cambridge, England)*, 126, 2911–2920. Available from: https://doi.org/10.1242/dev.126.13.2911

Ducy, P., Zhang, R., Geoffroy, V., Ridall, A.L. & Karsenty, G. (1997) Osf2/Cbfa1: a transcriptional activator of osteoblast differentiation. *Cell*, 89(5), 747–754. Available from: https://doi.org/10.1016/s0092-8674(00)80257-3

Edmund, A.G. (1960) *Tooth replacement phenomena in the lower vertebrates*. Toronto: Royal Ontario Museum. Available from: https://doi.org/10.5962/bhl.title.52196

Edmund, A.G. (1969) In: Gans, C. (Ed.) *Biology of the Reptilia, Part 1: Morphology A*. London: London Academic Press.

Fuenzalida, M., Illanes, J., Lemus, R., Guerrero, A., Oyarzn, A., Acua, O. et al. (1999) Microscopic and histochemical study of odontoclasts in physiologic resorption of teeth of the polyphyodont lizard, *Liolaemus gravenhorsti*. *Journal of Morphology*, 242, 295–309. Available from: https://doi.org/10.1002/(SICI)1097-4687(199912)242:3

Gaengler, P. (2000) Evolution of tooth attachment in lower vertebrates to tetrapods. In: *Development, function and evolution of teeth*. Cambridge: Cambridge University Press, pp. 173–185. Available from: https://doi.org/10.1017/CBO9780511542626.012

Garcia, M.A., Nelson, W.J. & Chavez, N. (2018) Cell–cell junctions organize structural and signaling networks. *Cold Spring Harbor Perspectives in Biology*, 10(4), a029181. Available from: https://doi.org/10.1101/cshperspect.a029181

Gonzalez Lopez, M., Huteckova, B., Lavicky, J., Zezula, N., Rakultsev, V., Fridrichova, V. et al. (2023) Spatiotemporal monitoring of hard tissue development reveals unknown features of tooth and bone development. *Science Advances*, 2, eadi0482. Available from: https://doi.org/10.1126/sciadv.adi0482

Hallett, S.A., Ono, W. & Ono, N. (2021) The hypertrophic chondrocyte: to be or not to be. *Histology and Histopathology*, 10, 1021–1036.

Handrigan, G.R., Leung, K.J. & Richman, J.M. (2010) Identification of putative dental epithelial stem cells in a lizard with life-long tooth replacement. *Development*, 137, 3545–3549. Available from: https://doi.org/10.1242/dev.052415

Handrigan, G.R. & Richman, J.M. (2010) Autocrine and paracrine shh signaling are necessary for tooth morphogenesis, but not tooth replacement in snakes and lizards (Squamata). *Developmental Biology*, 337, 171–186. Available from: https://doi.org/10.1016/j.ydbio.2009.10.020

Henriquez, J.I., Flibotte, S., Fu, K. & Richman, J.M. (2025) Molecular profiling of odontoclasts during physiological tooth replacement. *Journal of Dental Research*, 104, 561–571. Available from: https://doi.org/10.1177/00220345241304756

Holness, C.L. & Simmons, D.L. (1993) Molecular cloning of CD68, a human macrophage marker related to lysosomal glycoproteins. *Blood*, 81(6), 1607–1613.

14697580, 2026, 2, Downloaded from https://onlinelibrary.wiley.com/doi/10.1111/joa.70059 by Brno University Of Technology, Wiley Online Library on [31/03/2026]. See the Terms and Conditions (https://onlinelibrary.wiley.com/terms-and-conditions) on Wiley Online Library for rules of use; OA articles are governed by the applicable Creative Commons License

Howes, R.I. (1979) Root morphogenesis in ectopically transplanted pleurodont teeth of the iguana. *Cells, Tissues, Organs*, 103, 400–408. Available from: https://doi.org/10.1159/000145042

Huysseune, A. & Sire, J.-Y. (1997) Structure and development of teeth in three Armoured catfish, *Corydoras aeneus*, *C. arcuatus* and *Hoplosternum littorale* (Siluriformes, Callichthyidae). *Acta Zoologica*, 78, 69–84. Available from: https://doi.org/10.1111/j.1463-6395.1997.tb01128.x

Jiang, H., Sodek, J., Karsenty, G., Thomas, H., Ranly, D. & Chen, J. (1999) Expression of core binding factor Osf2/Cbfa-1 and bone sialoprotein in tooth development. *Mechanisms of Development*, 81, 169–173. Available from: https://doi.org/10.1016/S0925-4773(98)00232-9

Kavková, M., Šulcová, M., Dumková, J., Zahradníček, O., Kaiser, J., Tucker, A.S. et al. (2020) Coordinated labio-lingual asymmetries in dental and bone development create a symmetrical acrodont dentition. *Scientific Reports*, 10(1), 22040. Available from: https://doi.org/10.1038/s41598-020-78939-2

Kawasaki, K. (2009) The SCPP gene repertoire in bony vertebrates and graded differences in mineralized tissues. *Development Genes and Evolution*, 219, 147–157. Available from: https://doi.org/10.1007/s00427-009-0276-x

Kawasaki, K., Keating, J.N., Nakatomi, M., Welten, M., Mikami, M., Sasagawa, I. et al. (2021) Coevolution of enamel, ganoin, enameloid, and their matrix SCPP genes in osteichthyans. *IScience*, 24(1), 102023. Available from: https://doi.org/10.1016/j.isci.2020.102023

Kodama, J., Wilkinson, K.J., Iwamoto, M., Otsuru, S. & Enomoto-Iwamoto, M. (2022) The role of hypertrophic chondrocytes in regulation of the cartilage-to-bone transition in fracture healing. *Bone Reports*, 17, 101616. Available from: https://doi.org/10.1016/j.bonr.2022.101616

Komori, T., Yagi, H. & Nomura, S. (1997) Targeted disruption of Cbfa1 results in a complete lack of bone formation owing to maturational arrest of osteoblasts. *Cell*, 89(5), 755–764. Available from: https://doi.org/10.1016/s0092-8674(00)80258-5

LeBlanc, A.R.H., Brink, K.S., Cullen, T.M. & Reisz, R.R. (2017) Evolutionary implications of tooth attachment versus tooth implantation: a case study using dinosaur, crocodilian, and mammal teeth. *Journal of Vertebrate Paleontology*, 37(5), e1354006. Available from: https://doi.org/10.1080/02724634.2017.1354006

LeBlanc, A.R.H., Lamoureux, D.O. & Caldwell, M.W. (2017) Mosasaurs and snakes have a periodontal ligament: timing and extent of calcification, not tissue complexity, determines tooth attachment mode in reptiles. *Journal of Anatomy*, 231, 869–885. Available from: https://doi.org/10.1111/joa.12686

LeBlanc, A.R.H., Palci, A., Anthwal, N., Tucker, A.S., Araújo, R., Pereira, M.F.C. et al. (2023) A conserved tooth resorption mechanism in modern and fossil snakes. *Nature Communications*, 14(1), 742. Available from: https://doi.org/10.1038/s41467-023-36422-2

LeBlanc, A.R.H., Paparella, I., Lamoureux, D.O., Doschak, M.R. & Caldwell, M.W. (2021) Tooth attachment and pleurodont implantation in lizards: histology, development, and evolution. *Journal of Anatomy*, 238, 1156–1178. Available from: https://doi.org/10.1111/joa.13371

LeBlanc, A.R.H., Reisz, R.R., Brink, K.S. & Abdala, F. (2016) Mineralized periodontia in extinct relatives of mammals shed light on the evolutionary history of mineral homeostasis in periodontal tissue maintenance. *Journal of Clinical Periodontology*, 43(4), 323–332. Available from: https://doi.org/10.1111/jcpe.12508

Lian, J.B., Stein, G.S., Javed, A., Van Wijnen, A.J., Stein, J.L., Montecino, M. et al. (2006) Networks and hubs for the transcriptional control of osteoblastogenesis. *Reviews in Endocrine and Metabolic Disorders*, 7(1–2), 1–16. Available from: https://doi.org/10.1007/s11154-006-9001-5

Listgarten, M.A. & Shapiro, I.M. (1974) Fine structure and composition of coronal cementum in Guinea-pig molars. *Archives of Oral Biology*, 19(8), 679–696. Available from: https://doi.org/10.1016/0003-9969(74)90137-X

Liu, M., Reed, D.A., Cecchini, G.M., Lu, X., Ganjawalla, K., Gonzales, C.S. et al. (2016) Varanoid tooth eruption and implantation modes in a late cretaceous mosasaur. *Frontiers in Physiology*, 7, 145. Available from: https://doi.org/10.3389/fphys.2016.00145

Liu, W., Selever, J., Murali, D., Sun, X., Brugger, S.M., Ma, L. et al. (2005) Threshold-specific requirements for Bmp4 in mandibular development. *Developmental Biology*, 283, 282–293. Available from: https://doi.org/10.1016/j.ydbio.2005.04.019

Luan, X., Walker, C., Dangaria, S., Ito, Y., Druzinsky, R., Jarosius, K. et al. (2009) The mosasaur tooth attachment apparatus as paradigm for the evolution of the gnathostome periodontium. *Evolution and Development*, 11, 247–259. Available from: https://doi.org/10.1111/j.1525-142X.2009.00327.x

Luckett, W.P. (1993) Ontogenetic staging of the mammalian dentition, and its value for assessment of homology and heterochrony. *Journal of Mammalian Evolution*, 1, 269–282. Available from: https://doi.org/10.1007/BF01041667

McIntosh, J.E., Anderton, X., Flores-De-Jacoby, L., Carlson, D.S., Shuler, C.F. & Diekwisch, T.G.H. (2002) Caiman periodontium as an intermediate between basal vertebrate ankylosis-type attachment and mammalian 'true' periodontium. *Microscopy Research and Technique*, 59, 449–459. Available from: https://doi.org/10.1002/jemt.10222

Meunier, F.J. (2015) New data on the attachment of teeth in the angler fish *Lophius piscatorius* (Actinopterygii: Teleostei: Lophiidae). *Cahiers de Biologie Marine*, 2, 97–104.

Oddie, G.W., Schenk, G., Angel, N.Z., Walsh, N., Guddat, L.W., De, J. et al. (2000) Structure, function, and regulation of tartrate-resistant acid phosphatase. *Bone*, 27(5), 575–584. Available from: https://doi.org/10.1016/s8756-3282(00)00368-9

Otto, F., Thornell, A.P., Crompton, T., Denzel, A., Gilmour, K.C. & Rosewell, I.R. (1997) Cbfa1, a candidate gene for cleidocranial dysplasia syndrome, is essential for osteoblast differentiation and bone development. *Cell*, 89(5), 765–771. Available from: https://doi.org/10.1016/s0092-8674(00)80259-7

Palone, M., Casella, S., Bastianoni, D., Siciliani, G. & Lombardo, L. (2020) Lower incisor extraction therapy in a complex case with an ankylosed tooth in an adult patient: a case report. *International Orthodontics*, 18, 850–862. Available from: https://doi.org/10.1016/j.ortho.2020.08.006

Pautke, C., Tischer, T., Vogt, S., Haczek, C., Deppe, H., Neff, A. et al. (2007) New advances in fluorochrome sequential labelling of teeth using seven different fluorochromes and spectral image analysis. *Journal of Anatomy*, 210, 117–121. Available from: https://doi.org/10.1111/j.1469-7580.2006.00660.x

Pautke, C., Vogt, S., Tischer, T., Wexel, G., Deppe, H., Milz, S. et al. (2005) Polychrome labeling of bone with seven different fluorochromes: enhancing fluorochrome discrimination by spectral image analysis. *Bone*, 37, 441–445. Available from: https://doi.org/10.1016/j.bone.2005.05.008

Peyer, B. (1968) In: Zangerl, R. (Ed.) *Comparative Odontology*. Chicago: University of Chicago Press.

Rieppel, O. (2001) Tooth implantation and replacement in Sauropterygia. *PalZ*, 75, 207–217. Available from: https://doi.org/10.1007/BF02988014

Rieppel, O. & Kearney, M. (2005) Tooth replacement in the late cretaceous mosasaur Clidastes. *Journal of Herpetology*, 39(4), 688–692.

Rosa, J.T., Witten, P.E. & Huysseune, A. (2021) Cells at the edge: the dentin–bone Interface in zebrafish teeth. *Frontiers in Physiology*, 12, 723210. Available from: https://doi.org/10.3389/fphys.2021.723210

14697580, 2026, 2, Downloaded from https://onlinelibrary.wiley.com/doi/10.1111/joa.70059 by Brno University Of Technology, Wiley Online Library on [31/03/2026]. See the Terms and Conditions (https://onlinelibrary.wiley.com/terms-and-conditions) on Wiley Online Library for rules of use; OA articles are governed by the applicable Creative Commons License

Sahara, N., Ashizawa, Y., Nakamura, K., Deguchi, T. & Suzuki, K. (1998) Ultrastructural features of odontoclasts that resorb enamel in human deciduous teeth prior to shedding. *Anatomical Record*, 252, 215–228. Available from: https://doi.org/10.1002/(SICI)1097-0185(199810)252:2<215::AID-AR7>3.0.CO;2-1

Tan, W.H., Witten, P.E., Winkler, C., Au, D.W.T. & Huysseune, A. (2017) Telomerase expression in medaka (*Oryzias melastigma*) pharyngeal teeth. *Journal of Dental Research*, 96, 678–684. Available from: https://doi.org/10.1177/0022034517694039

Tong, A., Chow, Y.L., Xu, K., Hardiman, R., Schneider, P. & Tan, S.S. (2020) Transcriptome analysis of ankylosed primary molars with infraocclusion. *International Journal of Oral Science*, 12(1), 7. Available from: https://doi.org/10.1038/s41368-019-0070-1

Westergaard, B. & Ferguson, M.W.J. (1986) Development of the dentition in *Alligator mississippiensis*. Early embryonic development in the lower jaw. *Journal of Zoology*, 210, 575–597. Available from: https://doi.org/10.1111/j.1469-7998.1986.tb03657.x

Westergaard, B. & Ferguson, M.W.J. (1987) Development of the dentition in *Alligator mississippiensis*. Later development in the lower jaws of embryos, hatchlings and young juveniles. *Journal of Zoology*, 212, 191–222. Available from: https://doi.org/10.1111/j.1469-7998.1987.tb05984.x

Wu, X., Hu, J., Li, G., Li, Y., Li, Y., Zhang, J. et al. (2020) Biomechanical stress regulates mammalian tooth replacement via the integrin β1-RUNX2-Wnt pathway. *The EMBO Journal*, 39(3), e102374. Available from: https://doi.org/10.15252/embj.2019102374

Zaher, H. & Rieppel, O. (1999) Tooth implantation and replacement in squamates, with special reference to mosasaur lizards and snakes. *American Museum Novitates*, 3271, 1–19.

Zhu, D., Li, G., Fang, H. & Gao, Y. (2024) Emerging role of hypertrophic chondrocytes in tissue regeneration and fracture healing: a narrative review. *European Cells and Materials*, 47, 219–237. Available from: https://doi.org/10.22203/eCM.v047a14

SUPPORTING INFORMATION

Additional supporting information can be found online in the Supporting Information section at the end of this article.

How to cite this article: Šulcová, M., Dumková, J., Hutečková, B., Kavková, M., Parobková, V., Zahradníček, O. et al. (2026) Tooth–bone attachment tissue is produced by cells with a mixture of odontoblastic and osteoblastic features in reptiles. *Journal of Anatomy*, 248, 251–268. Available from: https://doi.org/10.1111/joa.70059

14697580, 2026, 2, Downloaded from https://onlinelibrary.wiley.com/doi/10.1111/joa.70059 by Brno University Of Technology, Wiley Online Library on [31/03/2026]. See the Terms and Conditions (https://onlinelibrary.wiley.com/terms-and-conditions) on Wiley Online Library for rules of use; OA articles are governed by the applicable Creative Commons License